

**FACULTY  
OF MATHEMATICS  
AND PHYSICS**  
Charles University

## **HABILITATION THESIS**

# **Stimulated inelastic interactions between free electrons and light**

RNDr. Martin Kozák, Ph.D.

Quantum Optics and Optoelectronics

Prague 2022



# Contents

Preface	1
1. Introduction: Motivation of the presented research	3
2. Stimulated inelastic scattering of electrons at optical fields	7
2.1. Introduction	7
2.2. Interaction of free electrons with optical near-fields	11
2.3. Interaction of free electrons with the ponderomotive potential of a travelling optical wave	16
2.4. Compression of electron pulses to attosecond durations	20
3. Studies of free electron-light interaction	23
3.1. Experimental setups	23
3.2. Overview of the results	27
4. Conclusion & outlook	31
Bibliography	32
Statement of the author's contribution to the publications	38
Appendix: Collection of publications	39

## Preface

In this habilitation thesis I present a collection of 15 papers with my co-authorship, which were published in international impacted journals during the years 2015-2021. These papers are cited in the text as references [A1-A15] (full bibliographic information is attached in the Appendix: Collection of publications). The works are focused on the experimental and theoretical research of the stimulated inelastic interactions between electrons freely propagating in vacuum and coherent optical fields of femtosecond laser pulses. The aims of the research are to control the electron beams on time scales of hundreds of attoseconds ( $1 \text{ as} = 10^{-18} \text{ s}$ ) and to accelerate the electrons to high energies using optical evanescent fields and optical ponderomotive forces. The presented results were obtained during my postdoctoral fellowship at Friedrich-Alexander-Universität Erlangen-Nürnberg in Germany during 2015-2017 and at the Faculty of Mathematics and Physics of Charles University during 2018-2021. Here I started to build an independent research group focused on the topics presented in this thesis and on ultrafast strong-field phenomena in solids driven by few-cycle laser pulses. I am the first and corresponding author of 11 papers of this collection and a sole author of 4 of them. I was involved in all the parts of these works including proposing the research directions, designing the experiments, their accomplishment, interpretation, numerical simulations and writing the manuscripts. The details of my contribution to these publications can be found in the Statement of the author's contribution to the publications, which is attached to this thesis.

The thesis is organized as follows: In chapter 1 I describe the motivation of the research together with a brief introduction. In chapter 2 I discuss the classical and quantum mechanical description of the inelastic interaction between free electrons and light fields in vacuum. In this chapter I also explain the principle of attosecond control of electrons and electron pulse compression to pulse durations below 1 femtosecond. In chapter 3 I describe the experimental setups and discuss the obtained results. In the final chapter 4 I present conclusions and a brief outlook for future directions in this research field.

This work would not be possible without a number of collaborators and colleagues. In particular I would like to thank prof. Petr Malý, doc. František Trojánek, prof. Petr Němec and other colleagues from the Department of Chemical Physics and Optics for their help, support and for creating nice and inspirative atmosphere. Further I would like to thank my postdoctoral adviser prof. Peter Hommelhoff from Friedrich-Alexander-Universität Erlangen-Nürnberg, who gave me a lot of freedom and great support during my postdoctoral fellowship in his group, where I spent 3 wonderful years. Some of the selected publications were produced in close collaboration with international partners, from which I list groups of R. L. Byer and J. S. Harris from Stanford University, CA, US and the group of I. Hartel from DESY in Hamburg, Germany. Also a number of PhD and master students have been involved in the laboratory work. I would also like to thank the grant agencies, namely to Gordon and Betty Moore Foundation, which supported the project ACHIP at which I took part during my postdoctoral fellowship, to Czech Science Foundation for the support of my junior research project "Ultrafast processes in solids controlled by few-cycle laser pulses" and to Charles University for the support via project PRIMUS with the title "Attosecond phenomena in solids".

Finally I also want to express my deepest thanks to my wife Petra and my whole family for their patience and great support.

# 1. Introduction: Motivation of the presented research

Physical and chemical properties of atoms and molecules are governed by the Coulomb interactions between fundamental constituents of matter, protons and electrons, which both carry electrical charge of opposite sign. Coulomb interaction together with quantum mechanical laws determine the shapes of atomic orbitals, electron energy structure and the interactions of atoms with the environment. The outermost electrons in the valence orbitals, which are relatively weakly bound, are responsible for chemical bonds and optical properties of matter. Therefore the possibility to directly observe valence electron orbitals and to take movies of electron wavepackets in motion is tempting and has many potential applications in the field of development of novel materials, chemistry or biophysics.

However, the spatial and temporal scales at which such dynamics occur, are extremely challenging to capture. When we consider a wavepacket generated as a coherent superposition of two stationary electronic states of a quantum system, its time evolution can be written as  $\psi(\mathbf{r}, t) = \exp(-iE_1 t/\hbar)\phi_1(\mathbf{r}) + \exp(-iE_2 t/\hbar)\phi_2(\mathbf{r})$ , where  $E_1$  and  $E_2$  are the energies of the two stationary states described by wave functions  $\phi_1(\mathbf{r})$  and  $\phi_2(\mathbf{r})$ . The probability of finding a quantum particle in a given point in space is determined by the square modulus of the wave function. This probability for the wavepacket corresponding to the two stationary states reads  $\rho(\mathbf{r}, t) = |\psi(\mathbf{r}, t)|^2 = |\phi_1(\mathbf{r})|^2 + |\phi_2(\mathbf{r})|^2 + \phi_1^*(\mathbf{r})\phi_2(\mathbf{r})\exp[-i(E_2 - E_1)t/\hbar] + c.c.$

Without dephasing, the wavepacket is characterized by harmonic oscillatory motion with the time period of  $T = 2\pi\hbar/|E_2 - E_1|$ . This characteristic time depends on the typical energy scale for the given quantum system. For molecular vibrations, the energies are of the order of 1-100 meV corresponding to oscillation periods of 20 fs - 2 ps. However, the energies of valence electronic states are of the order of 1-10 eV, which leads to typical time periods of about 200 as - 2 fs (1 fs=10<sup>-15</sup> s, 1 as=10<sup>-18</sup> s). Moreover, the spatial extent of the wave function of valence electron orbitals is several tens of picometers (1 pm=10<sup>-12</sup> m), which sets a stringent requirement for the spatial resolution needed to visualize such electronic wavepackets.

The first motivation of the research presented in this habilitation thesis is to develop experimental techniques allowing to image the coherent dynamics of valence electrons in solids driven by coherent light waves and the dynamics of the associated electromagnetic fields (optical near-fields, polarization waves, plasmons, etc.) with atomic spatial and sub-femtosecond temporal resolutions. Our approach is to use electron beams to probe the electromagnetic fields using new schemes of time-resolved electron microscopy, which has been developed during the last 20 years. In standard electron microscopy, a continuous beam of spatially coherent electrons accelerated to kinetic energies of many keV (typically 1-300 keV corresponding to de Broglie wavelengths of 2-40 pm) is used to illuminate the sample. While propagating through the sample, Lorentz force generated by the electrostatic fields of individual atoms in the sample is acting on the electrons and causes intensity and phase contrast in the electron wave, which can then be imaged with extremely high magnification on the detector. The record spatial resolution of less than 50 pm [1] allows to resolve individual atoms in a crystal lattice.

An extremely high spatial resolution of electron microscopes can be combined with time resolution by using pulsed electron beams, whose emission from a photocathode is controlled by short light pulses incident on the cathode surface. When

an ultraviolet (UV) pulse with photon energy higher than the material work function arrives to a metallic or semiconductor cathode in a microscope (typically tungsten, tungsten/ZrO<sub>x</sub> or LaB<sub>6</sub>), the temporal distribution of photoemitted electrons corresponds to the UV pulse envelope. The electrons are subsequently accelerated by the applied electrostatic field in the cathode region to the final kinetic energy of many keV. The generated electron pulses may serve for probing dynamical processes, which are typically triggered in the studied sample by excitation laser pulses coming in advance with a controlled time difference [2]. After the interaction with the sample, the electrons form either a direct image, then we talk about ultrafast electron microscopy, or a diffraction pattern in so-called ultrafast electron diffraction. These techniques have been applied to study the dynamics of chemical reactions [3], phase transitions [4] or magnetic field dynamics in nanostructures [5]. However, the best temporal resolution which can be obtained in these experiments is limited by the shortest achievable duration of the electron pulses at the location of the sample. The lowest pulse duration of electrons photoemitted by femtosecond laser pulses, which are not further compressed (the possibilities of post-compression are discussed in chapter 2.4.), is approximately 100-200 fs due to dispersive propagation of the electrons during their acceleration by the static electric field applied in the electron gun [6]. Because the natural length and time scales of electron wave packet dynamics in solids are picometers and attoseconds, ultrafast electron microscopy cannot resolve these dynamics nowadays. Our goals are to overcome this barrier and to compress the electron pulses to attosecond durations using the inelastic interaction with electromagnetic fields of femtosecond laser pulses. Such precisely controlled electron flashes may serve for experiments, in which the combination of extreme spatial and temporal resolutions is required.

Besides the control in the classical regime of the interaction, the electron matter waves can also be controlled in the quantum-coherent regime leading to generation of superposition of energy states separated by the photon energy of the driving light [7–11]. The quantum control of free electrons allows to study new types of coherent interactions between free electrons and matter [12] or using the free electrons as qubits for quantum simulations [13]. The complex spatio-temporal shaping of electron wavefunction by light may bring novel techniques and functionalities in electron microscopy and holography [14,15].

The second motivating factor for our research was to investigate a possibility to accelerate the electrons to high energies by light fields of low- or moderate intensities, which can be readily achieved in university-scale laboratories using amplified femtosecond laser systems. Such laser-driven electron accelerators may enable generation of coherent X-ray photons using free-electron laser (X-FEL) [16] schemes in much simpler and cheaper setups compared to the contemporary X-FEL facilities with hundreds of meters long accelerating structures [17]. It can also outperform the laser-driven plasma wakefield acceleration scheme [18], which requires extreme light intensities available only to large laser facilities [19]. The limiting factor of classical radio-frequency (RF) electron accelerators and the main reason, why their size cannot be easily reduced, is the maximum achievable energy gain of the electrons per unit length of the accelerating structure. This so-called accelerating gradient is physically limited to approx. 100 MeV/m by the maximum field, which can be applied to the internal surface of the RF cavities due to the electric breakdown phenomena [20]. The goal of laser driven particle accelerators based on optical near-fields is to increase the driving frequency by a factor of  $10^5$ - $10^6$  and in the same time to shrink down the size of the accelerating structure by the same factor.

Together with using periodic dielectric structures instead of metallic resonant cavities, this allows to increase the accelerating gradients to 1-10 GeV/m, which might potentially lead to reduction of the size of electron accelerators by a factor of 100x.

The first proposal of electron acceleration using optical near-fields (evanescent waves) has been published shortly after invention of laser [21,22]. In [22] the authors proposed to use a metallic grating with light incident perpendicular to the grating surface to accelerate electrons propagating along the direction of the grating vector. When the grating period is smaller than the wavelength of the incident light, classical diffraction of light in the far-field is not possible and the distribution of electromagnetic fields close to the grating surface can be written as a superposition of evanescent waves propagating along the surface. If the phase velocity of one of these waves is synchronized with the electron's propagation velocity, the electron gains or losses energy dependent on its phase relative to the synchronous wave. The experimental realization of this principle has waited until 2013, when two independent groups of researchers led by Prof. Byer at Stanford University [23] and Prof. Hommelhoff at Friedrich-Alexander-Universität Erlangen-Nürnberg [24] demonstrated its feasibility. Starting from these proof-of-principle experiments, the research in this field has focused to various aspects of the future laser-driven accelerators, which are the electron source [A2,A11], development of nanostructures with efficient coupling of light energy to the acceleration mode [A5,A12], use of novel materials [A14], steering and focusing electron optics driven by lasers [A4,A9] and electron diagnostics [A3].

In contrast to RF accelerators, the laser-driven particle accelerators have a disadvantage in the small effective volume of the accelerating fields. The evanescent nature of the optical near-fields leads to sub-wavelength decay length of the amplitude of the synchronous mode [25]. Moreover, the advantage of RF accelerators is that the electrons reach MeV energies corresponding to the velocity close to the speed of light  $c$  ( $v > 99\%$  of  $c$ ) within the first few periods of the accelerating structure, typically even in the electron gun. In contrast, the maximum energy gain per one period of the accelerating structure of optical near-field-based accelerators is about few hundreds of eV, which means that approximately  $10^4$  periods are needed to reach 1 MeV electron energy. Together with the small transverse size of the fields and the presence of transverse forces with similar amplitude as the accelerating forces, this makes the electron dynamics in the optical near-field very complicated and prevents to reach high average electron currents by this acceleration principle. The possible applications thus cover mainly the field of time- and spatially-resolved imaging experiments with electrons, where sub-femtosecond temporal resolution may be reached [A4,A8,7,26–29].

Besides the interaction of free electrons and light waves in vacuum, my research interests span over the field of nonlinear light-matter interaction in solid-state systems. The motivation of this research is to transfer concepts from attosecond physics in atoms to solids and to investigate novel schemes allowing to control electronic excitations in matter on sub-femtosecond time scales [30]. This research field was born around year 2000 after the development of the technology for stabilization of carrier-envelope phase of ultrashort laser pulses [31]. In the strong-field regime of electron excitation, an electron bound in an atom can tunnel through a barrier formed by the superposition of the binding potential and the electromagnetic potential of the laser field. The timing of such excitation can be controlled on time scales much shorter than the period of the driving light wave [30,32]. Many fascinating experiments demonstrating dynamical electronic processes occurring on time scales of



hundreds of attoseconds have been carried out in the last 20 years [33–39]. However, a practical application of such ultrafast processes in solids is lacking and requires to solve several physical problems, which prevent to develop electronics working at optical frequencies. The main problem is energy dissipation during nonlinear light-matter interaction, which arises from real population of excited state carriers generated in the conduction and valence bands of the material. One dissipation channel is carrier relaxation via phonon emission, the other is nonradiative recombination, which is also accompanied by transferring the energy to the crystal lattice. Therefore it is important to discover nonresonant processes, which lead to minimum excited state population but allow to control the optical properties of solids on time scales of few femtoseconds or faster [40,41]. During the last 4 years I developed a unique setup generating mid-infrared few-cycle laser pulses with stabilized carrier-envelope phase [42], which now serves for the research of strong-field optical phenomena in solids and high harmonic generation. Due to the fact that our research of this topic is still in its initial stage (8 publications in impacted journals in 2018-2021), I decided not to include the recent results from this research field in the thesis.

## 2. Stimulated inelastic scattering of electrons at optical fields

### 2.1. Introduction

In this chapter I summarize the fundamental principles and the theoretical description of inelastic synchronous interaction between free electrons and coherent optical fields in vacuum.

In the classical picture, an electron can be described as a point charged particle which is moving through electromagnetic fields oscillating at optical frequencies. When interacting with an optical plane wave in vacuum, the electron's acceleration/deceleration by the optical fields is prohibited by the so-called Lawson-Woodward's theorem [43,44]. This theorem assumes that: i) the interaction region is spatially infinite, ii) the electromagnetic wave is propagating in vacuum with no boundaries present, iii) the electron is highly relativistic ( $v \approx c$  along the acceleration path, where  $c$  is light speed in vacuum), iv) no static electric or magnetic fields are present, and v) nonlinear effects (e.g., ponderomotive and radiation reaction forces) can be neglected. When all these assumptions are valid, the electron oscillates in the real and momentum spaces, but the net energy change after an integer number of field oscillations is zero. To make the inelastic interaction possible, the system has to violate one of the assumptions of Lawson-Woodward's theorem. In this thesis I will discuss two approaches, namely the violation of the condition ii) by using optical near-fields in the vicinity of dielectric structures and the violation of v) by employing optical ponderomotive forces. In all discussed cases, also the condition iii) is not met because we study the interaction of light fields with sub-relativistic electrons with  $v \ll c$ .

In the first case of the interaction of electrons with optical near-fields, the electron propagates close to an object illuminated by a coherent light wave. In general, the optical near-field is generated when a plane wave scatters off an object with complex refractive index  $\tilde{n} \neq n_0$ , where  $n_0$  is the refractive index of a homogenous surrounding medium. The polarization induced by the object acts as a source of waves which interfere with the incident plane wave. When the object's dimensions are much smaller than the wavelength of the wave, the interference leads to a localized spatial modulation of the amplitude and phase of the electromagnetic wave. In general, the optical near-field can be decomposed to a sum of evanescent optical modes each of which is characterized by a phase velocity  $|\mathbf{v}_p^m| < c$  that can be matched to the electron propagation velocity for some particular mode with index  $m$ . The amplitudes of these synchronous modes decay rapidly with the distance from the object with sub-wavelength decay lengths.

When an isolated nanostructure is used, the effective length of the interaction of the electron with the field is limited to the near-field region. This length can be significantly increased by propagating the electrons along a flat structure with periodic modulation of the surface depth [24] or by using evanescent waves generated at a flat dielectric surface by total internal reflection [A5]. The interaction is only efficient when fulfilling a synchronicity condition between the electron propagation velocity and the phase velocity of the evanescent wave. For periodic structures, this condition arises from the spatial periodicity of the structure and the temporal symmetry of the optical wave. The electron needs to interact with the same phase of the periodic optical field at each period of the nanostructure leading to a condition for the initial electron

velocity  $v_0 = c\Lambda/\lambda$ , where  $c$  is speed of light in vacuum,  $\Lambda$  is the period of the nanostructure and  $\lambda$  is the wavelength of the light wave. In Fig. 1 I show the comparison of the classical interaction between an electron propagating at velocity  $v_0$  and optical fields of (a) an optical plane wave and (b) a synchronous optical near-field of a periodic nanostructure. Fig. 1a) and b) show the snapshots of the electric field component along the electron's trajectory  $E_z$  for two times  $t=0$  and  $t=T/2$ , where  $T$  is the period of the driving wave. In the case of the interaction with the plane wave, the field which the electron experiences along its trajectory is symmetric in time leading to zero net energy gain after an integer number of periods (black curve in Fig. 1c)). However, in the optical near-field of a nanostructure, the time symmetry of the Lorentz force acting on the electron is broken leading to a change of its kinetic energy after an integer number of optical periods (red curve in Fig. 1c)). The details of the electron scattering at optical near-fields are discussed in chapter 2.2.

In the second type of interaction, which we studied both theoretically and experimentally, the electrons scatter at the ponderomotive potential of an optical travelling wave (Fig. 1d), violation of the condition  $v$ ) of the Lawson-Woodward's theorem). The ponderomotive potential  $U_p = e^2 |\mathbf{E}|^2 / (4m\omega^2)$  corresponds to the time-averaged kinetic energy of the electron in an oscillating electromagnetic field [45]. Here  $e$  and  $m$  are the electron charge and mass,  $\mathbf{E}$  is the amplitude of electric field of the optical wave and  $\omega$  its angular frequency. If the field amplitude is spatially modulated, the gradient of the potential generates a force  $\mathbf{F}_p = -\nabla U_p$  pushing the particle out of the regions of high intensity. The highest intensity gradient is reached when two optical waves interfere and form an optical standing wave with a period corresponding to half of the wavelength of both waves. The interaction of electrons with such optical standing wave was proposed already in 1933 by Pyotr Kapitsa and Paul Dirac, who considered coherent electron diffraction at such periodic structure made of light [46]. Because of its extremely low probability when using incoherent light sources, its first observation had waited until the development of pulsed lasers with high peak intensities. The effect was first observed with atoms [47] due to the resonant enhancement of the ponderomotive interaction and later also with electrons [48–50], as originally proposed. This process can be understood as stimulated Compton scattering in which the electron absorbs a photon from one wave and in the same time emits a photon to the other wave [51]. When interacting with standing wave formed by photons with the same photon energy, only the transverse momentum component (component perpendicular to the electron propagation direction) of the electrons changes but the kinetic energy does not change. The manipulation with the kinetic energy and the longitudinal momentum component of the electrons is possible via the interaction with an optical travelling wave prepared by intersecting two light waves at different frequencies [52,53]. When the light beams cross the electron trajectory under specific angles, the ponderomotive force has the only component in the direction along the electron's trajectory and the velocity of the wave matches the initial velocity of the electrons [A7] (see Fig. 1d)). In such case, only the longitudinal component of the electron's momentum (component along the propagation direction) and in turn its kinetic energy are modulated.

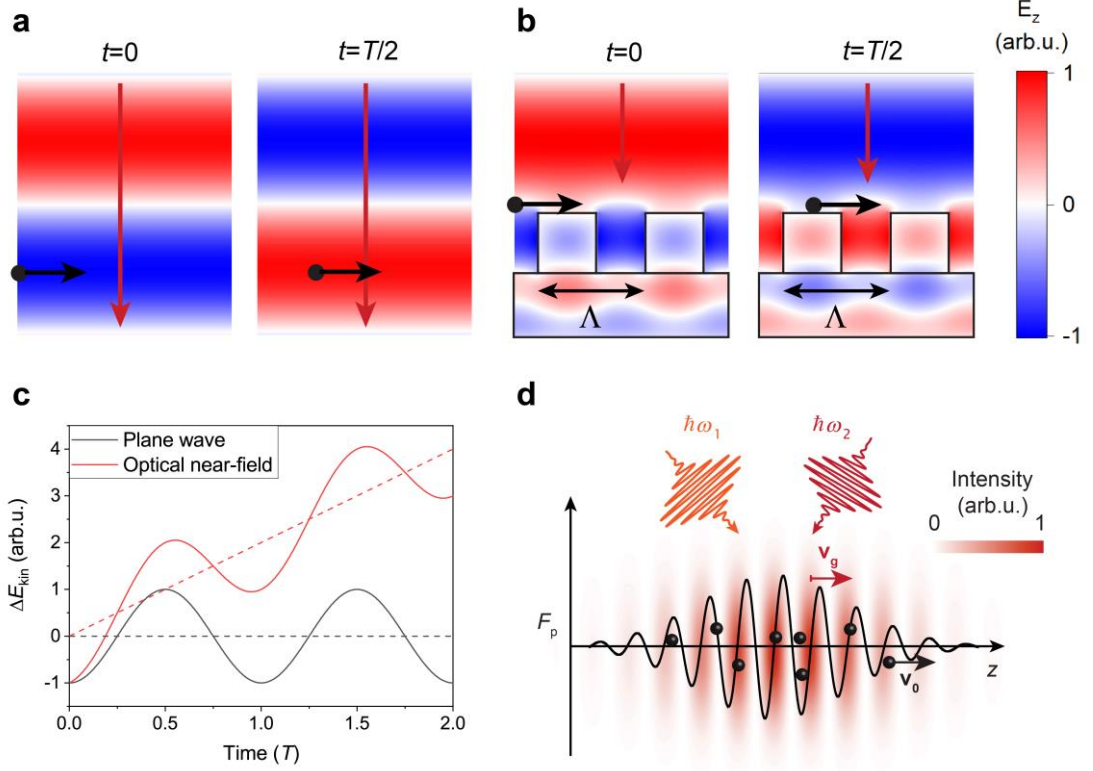


Fig. 1. An electron (black circle) propagating from left to right interacts with a) an optical plane wave and b) optical near-fields of a periodic nanostructure (silicon rectangular grating with period  $\Lambda$ ). The direction of the incident optical plane wave is shown by red arrows. The two snapshots of the distribution of optical fields in times  $t=0$  and  $t=T/2$  are shown ( $T$  is the temporal period of the optical wave). c) Kinetic energy of the electron as a function of time in the field of a plane wave (black curve) and synchronous optical near-field (red curve). d) Visualization of the interaction of electrons with the ponderomotive potential of an optical travelling wave formed by two laser beams with different photon energies  $\hbar\omega_1$  and  $\hbar\omega_2$ . The snapshot of the potential in the rest frame of the wave is shown (red color scale) together with the magnitude of the  $z$ -component of the ponderomotive force  $F_p$  (black curve) acting on the electrons in the direction of their propagation (adapted from [A7]).

The conditions for an efficient momentum transfer between photon and electron can be in both cases obtained in the particle picture by considering the momentum and energy conservation laws during an inelastic scattering event [A7]. Here we neglect spontaneous Compton scattering, which produces negligible change of the energy of the incident photon [54] and has very low probability at visible or infrared wavelengths [55]. When looking to dispersion curves (energy vs. momentum) of an electron and a photon in vacuum, we find that the slope is different for any electron energy (see Fig. 2). While the electron dispersion curve (dark grey curve in Fig. 2) is described by  $E = \sqrt{(pc)^2 + (m_0c^2)^2}$ , the photon dispersion  $E = pc$  is linear (red line in Fig. 2). This means that the energy and momentum conservation cannot be fulfilled in the same time for any electron energy and plane-wave photons cannot be absorbed by a free electron. In the case of optical near-fields, due to the spatial localization of the photons at scales  $\Delta z$  smaller than the wavelength, the momentum distribution  $\Delta p_z = \hbar \Delta k_z$  ( $k = 2\pi/\lambda$  is the wavevector and  $k_z$  is its  $z$  component) broadens

due to Heisenberg uncertainty principle and the interaction of the electron with a retarded photon (blue line in Fig. 2) becomes possible [56]. In the case of the ponderomotive interaction with an optical travelling wave, the potential is generated by two light waves at different frequencies propagating in different directions. For simplicity we assume here that the two waves propagate opposite to each other and one of them is propagating in the direction parallel to the electron's velocity. A single scattering event can be described by simultaneous absorption of a photon from one wave and stimulated emission of a photon in the second wave (see the lower inset of Fig. 2). Such stimulated Compton scattering allows both the energy and momentum to be conserved when the electron energy shift  $\Delta E = \hbar\omega_1 - \hbar\omega_2$  and the momentum change  $\Delta p = [\omega_1 - (-\omega_2)]\hbar/c = (\omega_1 + \omega_2)\hbar/c$  fulfill the relation:

$$\frac{\Delta E}{\Delta p} = \frac{dE}{dp} = \frac{p_0 c^2}{\sqrt{(p_0 c)^2 + (m_0 c^2)^2}}, \quad (1)$$

where  $p_0$  is the initial electron momentum.

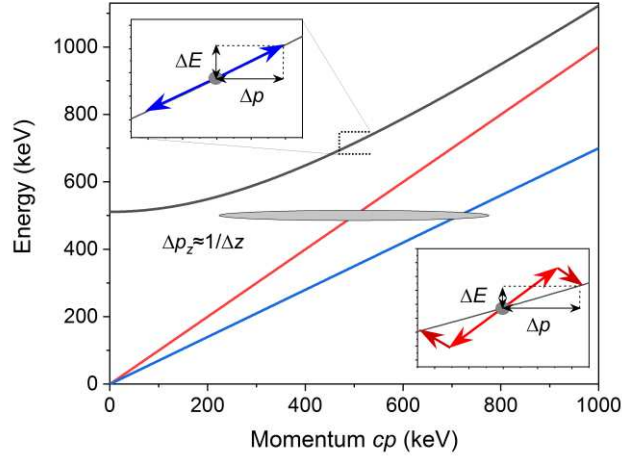


Fig. 2. Dispersion relations of a free electron (dark grey curve), free photon (red line) and a retarded photon (blue line). Upper inset: Conservation of energy and momentum during inelastic interaction of the electron with optical near-field. Spatial localization of the field causes its delocalization in the momentum space (grey ellipse) and allows to conserve the energy and momentum. Lower inset: The interaction of the electron with ponderomotive potential of an optical travelling wave formed by two counter-propagating light waves at different frequencies. One photon is absorbed from one wave while other photon is emitted to the other wave in a stimulated manner. For this reason, the electron energy shift after a single scattering event equals to the photon energy difference but the momentum change equals to the sum of the absolute values of the momenta of the two photons.

In the following two sections I discuss the theory of stimulated inelastic scattering of electrons at optical near-fields and at the ponderomotive potential of optical travelling waves in more detail. In general, the interaction can be described within three different approximations depending on the interaction regime:

1) Fully classical description using point particle approximation of the electron, which interacts with the classical light fields via Lorentz force. This approximation neglects the quantum nature of the electrons and light, but can successfully describe experiments with electron beams with limited coherence and also strong interaction regime, in which the electron dynamics during the interaction plays role.

2) Semiclassical approximation, in which the Schrödinger equation for an electron wavepacket is solved with the interaction Hamiltonian with classical vector potential describing the coherent light field. This approximation is required if the coherence time of the electrons is longer than the period of the driving light. In this case, the periodic phase modulation of the electron wavepacket leads to peaks in the electron spectrum corresponding to coherent absorption and emission of integer number of photons.

3) Fully quantum theory – typically not necessary because the driving light has a form of a coherent wave containing many photons (typically  $10^{10}$  or more) and absorption/emission of a small number of photons by the electron is not observable in the transmitted or reflected light.

I focus on the classical and semi-classical description of the interactions.

## 2.2. Interaction of free electrons with optical near-fields

The interactions of swift electrons with matter can be divided to two categories, spontaneous and stimulated. Spontaneous interactions correspond to a cases in which no external electromagnetic fields are present. The electron propagating close to a material generates various excitations (plasmons, plasmon-polaritons, phonons) via coupling of the evanescent field of the moving charge with polarization of the material [57]. The electron energy loss spectroscopy (EELS) of inelastically scattered electrons then serves for local probing of these excitation with sub-nanometer spatial resolution. Besides generating the real excitations, the electron can lose its energy via coherent or incoherent cathodoluminescence. Spectroscopy of cathodoluminescence photons carries information about, e.g., the density of localized plasmonic states of the sample [57]. Stimulated interactions involve external light in a form of a coherent wave illuminating the material through (around) which the electron propagates. The electron then interacts with the electromagnetic fields and coherent polarization in the material generated by this wave. When the electron does not propagate through the material but only in its vicinity, the effect of the stimulated interaction is typically much stronger than the spontaneous energy loss and the spontaneous effects can be neglected [58].

The first problem which has to be solved to describe the interaction of electrons with coherent optical near-fields is to find the expression for the spatial distribution of electric and magnetic fields in the vicinity of the illuminated nanostructure. This can be done analytically for a few basic shapes of the structures [57,59], but it is usually obtained by numerical solution of Maxwell's equations using boundary-element method [60] or finite-difference time domain (FDTD) method [61] for a nanostructure with a general shape. FDTD method is based on discretization of space and time coordinates. The initial conditions of the calculation are the spatial distribution of the complex dielectric constant defined by the shape of the nanostructure and its material and the initial spatial distribution of electromagnetic fields and their sources distributed on the discrete spatial mesh. The fields are then propagated in time by

integrating Maxwell's equations with respect to time using some form of Yee's algorithm [62]. By using physical constraints it is possible to optimize the geometrical shape of the nanostructures used for generation of the optical near-fields to provide optimal coupling of the incident light to the evanescent wave synchronous to the electrons. Such optimization using a commercial software Lumerical FDTD [63] was used to design the structures described in publications [A3,A6,A9,A11,A12].

The physics of the interaction of a charged particle (in our case an electron) with optical near-fields generated in a vicinity of a nanostructure has been discussed elsewhere [56,57]. In this work I focus mainly on periodic nanostructures which allow to enhance the coupling between light and electrons by extending the interaction distance. In the geometry assumed here (shown in Fig. 3a)), a periodic nanostructure is illuminated by coherent optical fields in a form of a plane wave. The  $k$ -vector of the driving light wave is typically perpendicular to the trajectory of the electron and the polarization of its electric field is parallel to the electron's propagation direction. The near-field distribution in the vicinity of the nanostructure is periodically modulated in space due to the contrast of dielectric constants of vacuum and the material used for the nanostructure fabrication. It is advantageous to describe the spatial distribution of the electric field amplitude in the optical near-field region using spatial Fourier transform as a superposition of infinite number of evanescent modes (spatial harmonics with integer index  $m$ ) propagating along the surface of the nanostructure with the phase velocities  $v_p^m = (c\Lambda)/(m\lambda)$ , where  $\Lambda$  is the spatial period of the nanostructure,  $\lambda$  is the wavelength of the driving light and  $m$  is the integer number index of the harmonics. Because the evanescent modes have to obey Maxwell's equations in vacuum, the transverse component of the wave vector is complex and the amplitudes of the synchronous waves decay exponentially with the distance from the nanostructure surface with a decay length of  $\delta = \lambda / \left( 2\pi \sqrt{c^2/v_p^2 - 1} \right)$  [25] (see Fig. 3b)).

If we assume synchronous interaction (the phase velocity of a particular evanescent mode  $v_p^m$  is equal to the initial velocity of the electron  $v_0$ ) and sub-relativistic electrons with energies 1-100 keV, the decay length  $\delta$  is much smaller than the wavelength of the driving light  $\lambda$ . This fact significantly limits the transverse spatial acceptance of the structures based on this principle to several hundreds of nanometers for optical drivers, which in turn limits the maximum achievable current of interacting electrons due to finite peak brightness of available electron sources [64,65].

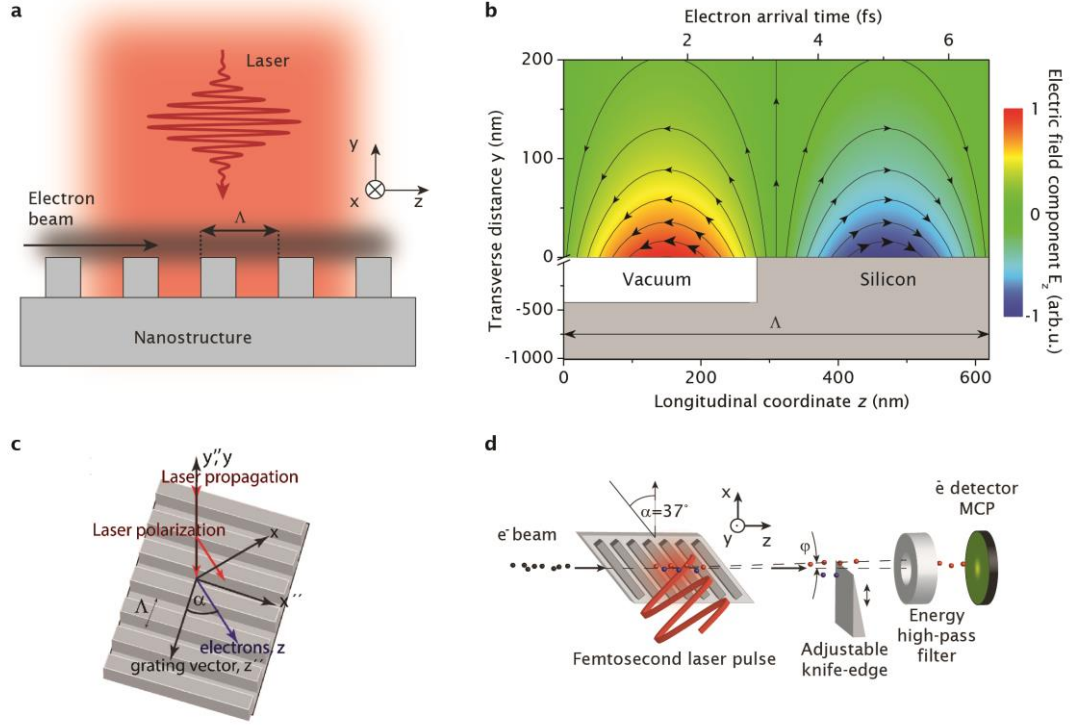


Fig. 3. a) Typical geometry used for inelastic electron interaction with optical near-fields of a periodic nanostructure. b) The color scale shows the snapshot of  $z$ -component of the electric field of the synchronous evanescent wave generated by light with wavelength  $1.93 \mu\text{m}$  synchronous with the electrons propagating at velocity  $v_0=0.32c$  at the surface of a silicon rectangular grating, which causes electron acceleration/deceleration. The arrows indicate the magnitude and direction of the electron's momentum change after the interaction as a function of its position with respect to the synchronous wave. c) A more complex geometry in which the grating vector is not parallel to the electron beam leading to generation of transverse forces in the plane of the nanostructure surface. d) Experimental geometry demonstrating the transverse streaking of the electrons [A4,A9].

We start with the classical description and assume that the electron propagates with velocity  $\mathbf{v}=(0,0,v_0)$  along the  $z$ -coordinate. If the relative change of the electron's velocity during the interaction is small ( $\Delta v \ll v_0$ ) and the electron propagates parallel to the surface of the periodic nanostructure, the electron feels a constant amplitude and phase of the field of the synchronous mode over the whole interaction. The final kinetic energy of the electron can be calculated as:

$$E_k = E_{k0} + \int_{-\infty}^{\infty} F_z(x, y, z, t) dz = E_{k0} - ev_0 \int_{-\infty}^{\infty} f(z, t) E_z(x, y, z') dt, \quad (2)$$

where  $E_{k0} = 1/2 m_0 v_0^2$  is the initial kinetic energy of the electron,  $E_z(x, y, z') = E_0(x) \exp(-\delta y) \sin(2\pi z'/\Lambda)$  is the  $z$ -component of the oscillating part of the electric field (component along the electron trajectory) of the synchronous evanescent wave in the electron rest frame characterized by Galilean transformation  $z' = z - v_0 t, x' = x, y' = y, t' = t$  and  $f(z, t)$  is the time envelope of the electric field given by the pulsed nature of the driving light and its spatial distribution in the



laboratory frame. We assume slowly varying envelope approximation, in which the changes of  $f(z,t)$  are small at time and spatial scales given by the period and wavelength of the driving light. The electric field of each spatial harmonics with phase velocity different from  $v_0$  is a harmonic function of time in the electron's rest frame and the integral in Eq. (2) yields zero value and the only nonzero contribution arises from the synchronous mode. The amplitude of the synchronous mode  $E_0(x)$  is obtained numerically and depends on the material and shape of the nanostructure. The magnetic part of the Lorentz force  $\mathbf{F}_L = q(\mathbf{E} + \mathbf{v} \times \mathbf{B})$  can be neglected as it acts in the direction perpendicular to the electron's velocity and thus causes only electron deflection but no change of the electron's kinetic energy.

Because the electric field of the synchronous wave is stationary in the rest frame of the electron, the spatial dependence of the kinetic energy modulation has the same form as  $E_z$ . By transforming back to the laboratory frame using  $z = z' + v_0 t$  we find that the kinetic energy of a beam consisting of moving electrons randomly distributed in the direction of their propagation is harmonically modulated in time. The final electron energy and momentum change is determined by the injection phase to the synchronous wave (initial electron position in the rest frame  $z'_0$ ), as shown in Fig. 3b). If a continuous stream of electrons is injected to such photonic accelerator, the electron spectrum broadens because the electrons scan all the phases of the driving field [23,24]. A measured spectrum of electrons interacting with optical near-field generated by mid-infrared femtosecond laser pulses at the surface of silicon nanograting is shown in Fig. 4 (red curve) together with numerical simulation (black dashed curve). The simulated spectrum was obtained using an ensemble of  $10^5$  electrons with Gaussian distributions in space and time domains corresponding to the pulsed electron beam used in the experiment [A11].

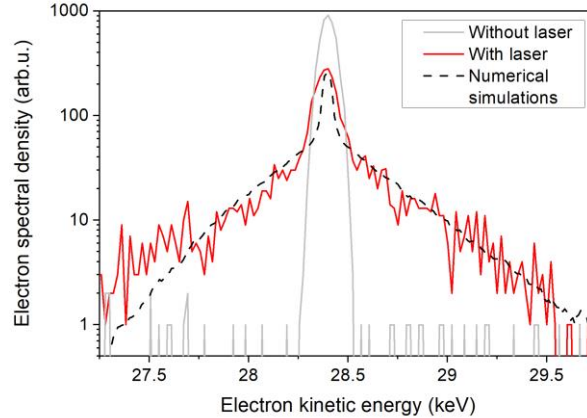


Fig. 4. Measured energy spectra of electrons propagating close to a periodic silicon nanograting with (red curve) and without (grey curve) the presence of driving laser fields. The pulsed electron beam with pulse duration of  $\tau=410$  fs (full-width at half maximum) was focused to a spot size of  $w_0=50$  nm ( $1/e^2$  radius) and its center was 100 nm above the grating surface. The interaction was driven by laser pulses with duration of approx. 100 fs and center wavelength of 1930 nm. Part of the electron distribution does not interact with the laser pulse due to limited temporal overlap of the electron and laser pulses at the nanostructure (for details see [A11]).

When a device should provide only acceleration, the electron injection time with respect to the phase of the accelerating optical field have to be precisely controlled. However, due to the typical time period of electromagnetic fields at optical frequencies of few femtoseconds, the time window for electron acceleration is only few hundreds of attoseconds within each optical period of the synchronous mode. This is one of the drawbacks of the proposed accelerators based on optical near-fields. To allow acceleration of a significant fraction of the incident continuous electron beam, the electrons have first to be compressed in time domain (the compression principle is explained in chapter 2.4).

Besides the force acting on the electrons in the direction of their propagation, there are also transverse components of the Lorentz force, which cause the deflection of the electrons. The transverse momentum transferred to the electron by the synchronous near-field can be calculated as  $\Delta\mathbf{p}^\perp = \int_{-\infty}^{\infty} \mathbf{F}_L^\perp(t) dt$ , where  $\mathbf{F}_L^\perp(t)$  is the vector containing only the components of the Lorentz force perpendicular to the electron propagation direction. These forces exist naturally in any optical near-field due to the fact that the amplitudes of the electric and magnetic fields are modulated at shorter distances than the wavelength of the driving light. In the standard geometry shown in Fig. 3a), the only nonzero transverse component of the force is  $F_y$  because the structure is virtually infinite in the  $x$ -direction. In the case of a more general interaction scheme shown in Fig. 3c), there are also nonzero  $x$ -components of the Lorentz force [25], which can be used to streak [A4] or focus [A9] the electron beam.

In the case of a large change of the electron's energy already during the interaction (the approximation of the small velocity change is not valid), the full electron dynamics has to be described numerically by integrating the relativistic equation of motion with the Lorentz force  $d(\gamma m_0 \mathbf{v})/dt = q(\mathbf{E} + \mathbf{v} \times \mathbf{B})$ , where

$\gamma = \sqrt{1 - |\mathbf{v}|^2/c^2}^{-1}$  is the relativistic Lorentz factor,  $\mathbf{v}$  is electron velocity,  $m_0$  is the rest mass of electron,  $c$  is speed of light and  $\mathbf{E}$  and  $\mathbf{B}$  are the space- and time-dependent amplitudes of the electric and magnetic fields, respectively.

The semiclassical description of the interaction in the approximation of negligible velocity change of the electrons and no recoil (absorption of photons from the driving wave can be neglected) can be formulated using path integral representation of the wave function, where the quantum mechanical phase acquired by the electron along a classical trajectory can be written as [66]:

$$\Phi(\mathbf{r}, t) = -\frac{1}{\hbar} \int_{t_0}^t H_{\text{int}}[r(t'), t'] dt', \quad (3)$$

where the interaction Hamiltonian  $H_{\text{int}} = (\hat{\mathbf{p}} + e\mathbf{A})^2/2m_0$  and  $r(t')$  is the classical electron trajectory. Here  $\mathbf{A}$  is the vector potential of the electromagnetic field, which in Coulomb gauge fulfils the calibration condition  $\nabla \cdot \mathbf{A} = 0$  and which is related to the electric field by  $\mathbf{E} = -\partial\mathbf{A}/\partial t$ , and  $\hat{\mathbf{p}}$  is momentum operator. In the case of the interaction of the electron with electromagnetic fields in vacuum (without a presence of a nanostructure), the part of the interaction Hamiltonian linear in the field cancels out due to the mismatch of the propagation velocity of the electron and the phase velocity of light. In the first order perturbation, the phase changes of the wave function acquired during the positive and negative parts of the field oscillations exactly cancel out. However, when a synchronous evanescent wave is present, the interaction

Hamiltonian for harmonic driving wave can be approximated (we neglect the term quadratic in vector potential) as  $H_{\text{int}} = e\hat{\mathbf{p}}\mathbf{A}(\mathbf{r}, t)/m_0$  and the phase of the electron wave function is harmonically modulated at the frequency of the driving light. The phase modulation of the electron wave function from Eq. (3) reads:

$$\Phi(\mathbf{r}, t) = 2|g| \sin[\omega z'/v_0 + \arg(g)]. \quad (4)$$

Here  $g = e/2\hbar\omega \int_{-\infty}^{\infty} E_z(x, y, z) e^{-i\omega z/v_0} dz$  describes the strength of the electron-light interaction. When assuming the initial electron wave function in the form of a plane wave (the wavefunction normalization can be done by introducing a finite envelope function), the final state with the harmonic phase modulation can be written as a superposition of plane-waves as [7,29,59]:

$$\Psi_{\text{out}}(x, y, z, t) = \sum_{n=-\infty}^{\infty} J_n(2|g|) \exp\left\{ \frac{i}{\hbar} \left[ \left( p_0 + \frac{n\hbar\omega}{c} \right) z - (E_{k_0} + n\hbar\omega) t \right] + in \arg(-g) \right\}, \quad (5)$$

where  $J_n$  is the  $n$ -th order Bessel function of the first kind and  $p_0 = m_0 v_0$  is the initial electron momentum. The resulting electron wave function consists of states shifted in energy by the photon energy of the driving wave  $\hbar\omega$ . The probability of transition to the  $n$ -th state is given by  $P_n = J_n(2|g|)^2$ . The probability is thus an oscillatory function of the interaction strength  $g$  leading to oscillating populations of individual photon sidebands as a function of the field strength of the driving light observed in the quantum coherent regime of the interaction [7].

If the approximations of no recoil and of negligible change of the electron momentum during the interaction are not met, the interaction can be described using numerical solution of Schrödinger equation [67].

### 2.3. Interaction of free electrons with the ponderomotive potential of a travelling optical wave

The second approach allowing to modulate the kinetic energy of electrons by light discussed in this thesis is based on the interaction, which was proposed already during the early stages of quantum mechanics. Kapitsa and Dirac suggested that if an electron matter wave propagates through an optical standing wave formed by two counterpropagating optical beams, the electron wavepacket would coherently diffract [46,51]. The interaction is mediated by the so-called ponderomotive potential which arises from the fact that a charged particle in oscillating electromagnetic fields acquires additional kinetic energy due to its oscillatory motion. If we assume that a charged particle is initially in rest, the force induced by a harmonic electromagnetic wave can be expressed as  $F = qE \cos(\omega t)$  (we neglect the magnetic part as it is usually sufficiently weak for initial electron velocity  $v_0=0$  and sub-relativistic field amplitudes), where  $q$  is the electric charge of the particle,  $E$  and  $\omega$  are the amplitude and frequency of the optical field. After integrating the equation of motion one obtains the velocity of the particle  $v = qE \sin(\omega t)/\omega m_0$  and the instantaneous kinetic energy can be written as  $E_k = q^2 E^2 \sin^2(\omega t)/(2\omega^2 m_0)$ , where  $m_0$  is the particle mass. The

ponderomotive energy corresponding to the time average of the kinetic energy thus can be expressed as  $U_p = \langle E_k \rangle = q^2 E^2 / (4m_0 \omega^2) = q^2 I / (2\varepsilon_0 c m_0 \omega^2)$ , where  $I$  is the intensity of the incident light and  $\varepsilon_0$  is the vacuum permittivity. When the light intensity is constant in space, the ponderomotive potential is also constant and there is no associated force acting on the particle. However, when the intensity is spatially modulated, the ponderomotive force  $\mathbf{F} = -\nabla U_p = -\nabla |\mathbf{E}|^2 q^2 / (4m_0 \omega^2)$  pushes the particle out of the high intensity regions. An interesting property of this force is the fact that due to the quadratic dependence on the electric charge it acts on the particles with both signs of the charge in the same way.

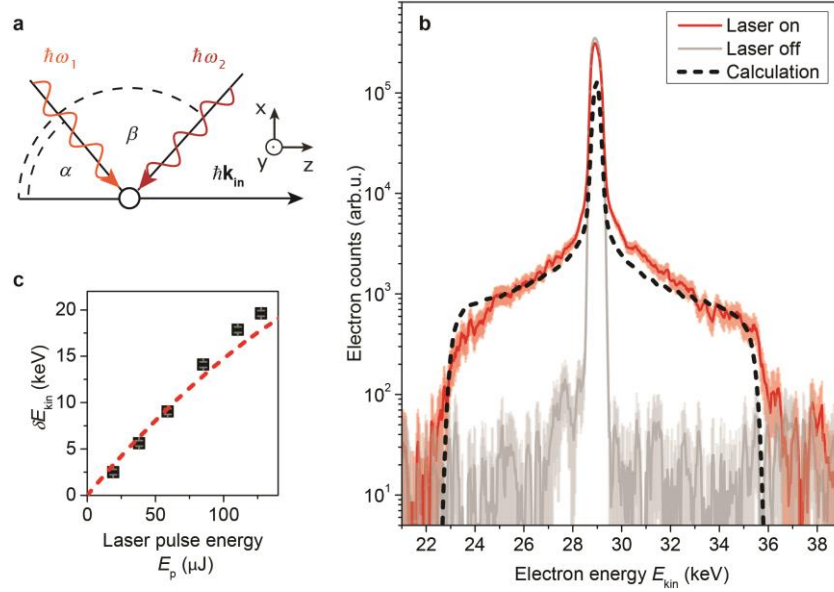


Fig. 5. a) Geometry of the generation of optical travelling wave propagating synchronously to an electron (circle) moving from left to right. b) Electron spectrum after the interaction with laser beams (red curve) compared to spectrum without the presence of laser fields (grey curve). c) Measured (squares) and calculated (dashed line) final spectral width of the electron distribution after the interaction as a function of pulse energies of each of the two driving pulses.

To generate a constant force acting on moving electrons along their trajectory we need to create a gradient of light intensity, which is not stationary but has a form of a travelling wave. Such wave can be generated by two electromagnetic waves at different frequencies  $\omega_1$  and  $\omega_2$ , which are intersected with the electrons under angles  $\alpha$  and  $\beta$  (see the scheme in Fig. 5a)) [A7]. The total electric field is obtained as superposition of the two fields (we assume plane waves for simplicity) and the ponderomotive potential can be written as:

$$U_p = \frac{e^2}{2m_0 \omega_1 \omega_2} \times \left( |E_{10}|^2 + |E_{20}|^2 + E_{10} E_{20} \cos \left\{ -i \left[ (\omega_1 - \omega_2) t - (\omega_1 \cos \alpha - \omega_2 \cos \beta) \frac{z}{c} - (\omega_1 \sin \alpha - \omega_2 \sin \beta) \frac{y}{c} \right] \right\} \right), \quad (6)$$

Here  $E_{10}$  and  $E_{20}$  are the amplitudes of the two optical waves. We assume that both polarizations are perpendicular to the plane defined by the two optical beams and the electron beam. Eq. (6) does not take into account relativistic effects and is valid only for Lorentz factor  $\gamma \approx 1$ . The velocity of the wave in the laboratory frame is  $v_w = (\omega_1 - \omega_2)c / (\omega_1 \cos \alpha - \omega_2 \cos \beta)$  [A7]. When an electron propagates through the optical wave with the same velocity  $v_0 = v_w$ , the potential becomes stationary in the rest frame of the electron. When we again assume the condition of negligible velocity change during the interaction, the final kinetic energy can be expressed as:

$$E_k = E_{k0} - v_0 \int_{-\infty}^{\infty} f(z, t) \nabla_z U_p(x, y, z') dt, \quad (7)$$

where  $z' = z - v_w t$  is the coordinate in the rest frame of the wave after Galilean transform and  $f(z, t)$  is an envelope function describing the spatial and temporal distribution of the ponderomotive potential. The resulting energy modulation is a harmonic function of  $z'$  similar to the case of optical near-fields. However, there is one significant difference between these two types of interactions which lies in the possibility to completely avoid transverse forces acting on the electrons in the case of the ponderomotive interaction. When the electrons are injected with random phases with respect to the travelling wave (their initial distribution in  $z'$ -coordinate is random), the electron spectrum after the interaction becomes broadened. This is shown in Fig. 5b), where we show a comparison of the electron spectrum with/without the presence of the optical travelling wave. The measurements were obtained using the time-resolved electron microscope setup, which is described in detail in chapter 3.1. In Fig. 5c) we plot the measured values of the final energy width of the electron distribution as a function of the pulse energies (proportional to peak intensities) of two pulses driving the interaction (black squares) compared with numerical simulations (dashed curve) [A7]. While the strength of the interaction scales linearly with  $|E_z|$  for the interaction with optical near-fields, the strength of the ponderomotive interaction is proportional to  $|E|^2$ .

The semi-classical description of the interaction is required when the coherence length of the electron wavepacket is comparable or longer than the spatial period of the optical travelling wave. The description is similar to the case of the optical near-fields. The quantum mechanical phase accumulated along a classical electron trajectory due to the presence of the optical fields can be expressed using Eq. (3) using the interaction Hamiltonian  $H_{\text{int}} = (\hat{\mathbf{p}} + e\mathbf{A})^2 / 2m$ . In this case, the part of the Hamiltonian linear in the vector potential cancels out due to the mismatch of the propagation velocity of the electron and the phase velocity of light. The only term leading to nonzero phase modulation is quadratic in the vector potential. The interaction Hamiltonian averaged over one period of the oscillating field has a form:

$$H_{\text{int}} = \frac{e^2}{2m} \langle |\mathbf{A}|^2 \rangle = \frac{e^2}{4m} |\mathbf{A}|^2 = \frac{e^2}{4m\omega^2} |\mathbf{E}|^2. \quad (8)$$

If we assume the light fields in the form of counter-propagating plane waves with the temporal envelope functions  $f(t)$  (generalization to nonzero angles of incidence  $\alpha$  and  $\beta$  can be obtained numerically [A7]), the spatially-dependent part of the ponderomotive potential of two counterpropagating beams generating a travelling wave synchronous to the electrons can be expressed as:

$$U_p = \frac{e^2 E_0^2}{4m\omega_1\omega_2} f\left(t - \frac{z'}{c} - \frac{v_0}{c}t\right) f\left(t + \frac{z'}{c} + \frac{v_0}{c}t\right) \exp\left[i\frac{\omega_1 + \omega_2}{c}z'\right] + c.c. \quad (9)$$

The electron wave function after the interaction obtains harmonic phase modulation (Fig. 6b)). Similar to Eq. (5) it can be written as a superposition of states with kinetic energy shifted from the initial state by  $n\hbar(\omega_1 - \omega_2)$ , where  $n$  is integer number [7]. The interaction thus acts as a coherent beamsplitter, which splits the initial electron state to a coherent superposition of states with different momenta (see Fig. 6c)). Such coherently prepared superposition of free electron states may find applications in new types of holographic imaging with electrons [68] or in quantum-optical experiments with electron wavepackets [9,12,13,27,69].

To observe the quantum signatures of the interaction, the spectral width of the initial electron distribution has to be smaller than the energy difference between the two neighbouring photon orders  $\hbar(\omega_1 - \omega_2)$ . This condition can also be expressed using the coherence time of the electrons, which has to be longer than the time period of the modulation  $T = 2\pi/(\omega_1 - \omega_2)$ . When this condition is met, the interaction can be described as diffraction in the time domain, during which parts of the electron wavepacket interacting with subsequent periods of the optical wave interfere. The constructive interference of waves with particular de Broglie wavelength leads to the peaks in the final electron spectrum while the destructive interference causes suppression of population between the peaks.

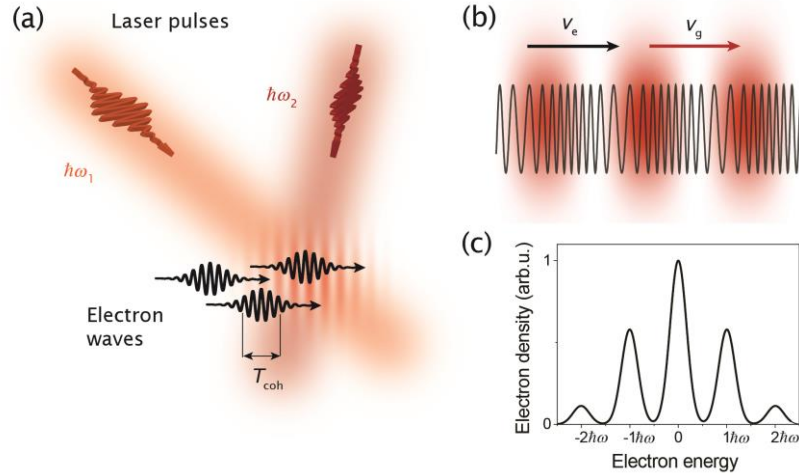


Fig. 6. a) Layout of the experiment for quantum-coherent modulation of electron waves by ponderomotive potential of an optical travelling wave in vacuum. b) Schematic picture of the electron phase modulation induced by the ponderomotive interaction with the synchronous travelling wave, which is stationary in the electron rest frame. c) Resulting electron spectrum after the interaction, which contains peaks separated in energy by the difference of the photon energies of the two light waves  $\hbar\omega = \hbar(\omega_1 - \omega_2)$ . The initial spectrum corresponds to the central peak. Here we assume a finite coherence length of the interacting electron wavepacket, which leads to broadening of the peaks in comparison with infinitely coherent plane wave, which would lead to a series of delta functions.

## 2.4. Compression of electron pulses to attosecond durations

In this chapter I show that besides the modulation of electron spectra, the interaction with optical fields allows to reach precise control of the temporal structure of the electron distribution and the arrival time of electron pulses to the experiment on sub-femtosecond time scales.

Compression of electron pulses, similar to optical pulses, is a two-step process. First, a time-correlated energy modulation is imprinted to the pulse. In optics this is typically done by self-phase modulation of an optical pulse propagating through a medium with third-order optical nonlinearity [70]. In the case of electrons, the energy modulation is a consequence of the interaction with light waves. The second step in optical pulse compression is compensation of dispersion using prism or grating compressors [71] or chirped mirrors [72], which allow to adjust all the frequency components of the pulse to be in phase. Because of a narrow relative energy spread of electron pulses after the interaction with light fields (typically  $\Delta E_k/E_k \sim 10^{-2}-10^{-3}$ ), the dependence of the group velocity of the electrons on the kinetic energy can be approximated as linear. For a fraction of the electrons, the harmonic velocity modulation can be approximated by a linear dependence (velocity linearly increasing with time, see red dashed line in Fig. 7) with slower electrons at the leading edge and faster electrons at the trailing edge. This part of the electron distribution becomes compressed and forms a short pulse after a certain propagation distance. The compression factor depends on the initial energy spread and the amount of chirp introduced to the electrons but it is possible to generate hundreds of attoseconds long pulses [A8]. I note that the duration of the compressed electron pulse is usually far from the limit given by the Heisenberg uncertainty relations between time duration and energy width  $\Delta t \Delta E \geq \hbar/2$  due to the limited longitudinal coherence of the electrons [6].

For compression using radiofrequency (RF) or terahertz (THz) fields, the minimum pulse durations demonstrated experimentally are  $\tau_{\text{FWHM}}^{\text{RF}} = 10$  fs [73] and  $\tau_{\text{FWHM}}^{\text{THz}} = 75$  fs [74]. However, the electronics generating the RF fields for the compression brings additional timing jitter, which is of the order of few femtoseconds. For reaching attosecond pulse durations and arrival time precision, all-optical schemes have to be applied. Here the timing jitter is much lower (attosecond level) because the relative time difference between the pulses is stabilized mechanically by optical path lengths of different laser beams in the experiment. Because light needs 3.3 attoseconds to pass a distance of 1 nanometer, mechanical vibrations have to be minimized.

The principle of compression of electron pulses and generation of attosecond spikes in the temporal probability distribution in the classical regime of the interaction is shown in Fig. 7. The initial electron distribution in time and momentum spaces is shown in the left two panels. Right after the interaction with optical fields, the velocity of the electrons acquire sinusoidal modulation in time reflecting the shape of the interaction potential, but the density distribution does not change (in the approximation  $\Delta v \ll v_0$ ). After propagating by a distance  $f_l$  corresponding to temporal focal length, the electron distribution in momentum space rotates due to the dispersive propagation in vacuum and forms vertical lines. The temporal density of the electrons at this point in space contains short spikes with sub-femtosecond durations, which are regularly spaced by the temporal period of the optical wave introducing the velocity modulation. The spikes are formed by the electrons with approximately linear velocity chirp ( $\Delta v_z / \Delta t = \text{konst}$ , red dashed line in Fig. 7). The compressed electrons thus contain

only about 30% of the electrons from the initial distribution [A8]. The rest of the particles is distributed around the peak and forms a background, which complicates the experiments with such electron pulse trains.

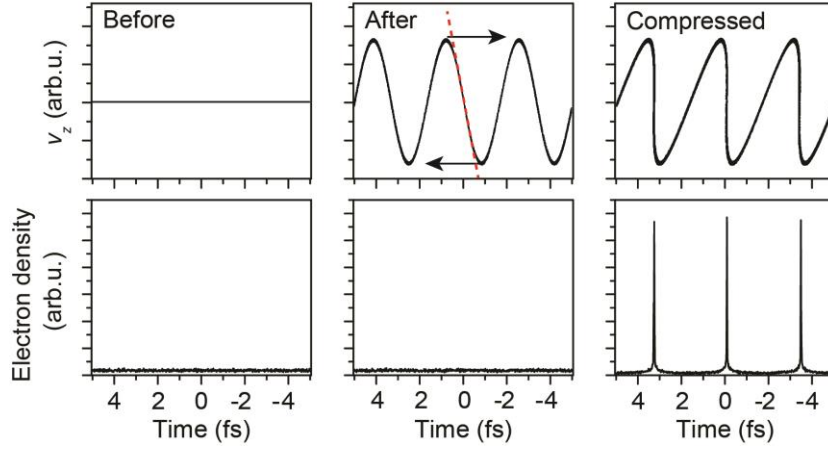


Fig. 7. The principle of electron pulse compression using optical fields. The upper panels show the velocity of the electrons as a function of time while the lower panels show the electron density in three different spatial locations along the electron beam path, namely before the interaction with optical fields, right after the interaction and after propagation over a drift distance required for ideal temporal focusing. The time displayed on  $x$ -axis refers to the time delay with respect to the center of the electron distribution. The red dashed line shows the part of the modulated electrons with approximately linear chirp.

The propagation distance  $f_t$  needed for ideal electron compression can be expressed using the initial electron velocity  $v_0$  and the magnitude of the linear energy chirp imprinted to the electrons  $dE_k/dt = \kappa = \Delta E_{\max}(t)(\omega_1 - \omega_2)$  as  $f_t = \gamma^3 m_0 v_0^3 / \kappa$  [A8]. The coefficient  $\kappa$  characterizes the strength of the light-electron interaction and can be controlled by the intensities of the light fields modulating the electron energy and other experimental parameters.

This compression principle works similarly for all the possible types of inelastic electron scattering induced by light fields, namely the interaction with optical near-fields [7,9,26], with semi-infinite fields of thin membranes [28,75] and with the ponderomotive potential of optical travelling waves [A8]. However, different schemes have different advantages and disadvantages for potential applications of the compressed electron pulse trains. In the case of optical near-fields, the strongest disadvantage is the sub-wavelength transverse spatial decay of the accelerating fields and the presence of phase-shifted transverse forces acting on the electrons during the modulation. This puts extremely high requirements for the quality of the electron beam, which has to be focused ideally to single nanometer spot sizes. The advantage of this interaction is very strong coupling of incident light with the electrons, which can be reached by optimized nanostructures with extended interaction distances [76] or by using resonant photonic cavities [10,77–79]. In the case of semi-infinite fields generated at dielectric or metallic membranes [28,75], the electrons have to propagate through the material of the membrane leading to electron scattering and loss of the beam current. Both the optical near-fields and semi-infinite fields are generated at nanostructures, which need to be illuminated by high-power light. The illumination by light with high peak intensity together with the impact of the electron beam usually



leads to slow degradation of the structures. These problems are not present in the third interaction scheme with the ponderomotive potential of a travelling optical wave. Here the interaction occurs in vacuum and no structure is required. Another advantage of the ponderomotive technique is the possibility to completely avoid transverse forces causing the electron deflection. On the other hand, the ponderomotive interaction is weak due to its dependence on the second power of the field and in general requires higher peak intensities of the driving light.

The electron pulses compressed using optical fields were recently applied to study the attosecond dynamics during electron diffraction at a sample illuminated by a light wave, which is coherent with the wave used for electron energy modulation [28]. By this method it is in principle possible to reach attosecond temporal and sub-nanometer spatial resolution in the ultrafast imaging experiments.

## 3. Studies of free electron-light interaction

### 3.1. Experimental setups

One of the motivating factors of our research is to develop new schemes allowing to accelerate electrons to high energies via the interaction with optical near-fields. Because the transverse decay of the field amplitude is shorter than the wavelength of the driving light, the experiments require tightly focused electron beams to make sure that the electrons are spatially overlapped with the optical near-fields. This is the main reason why all the experiments with slow electrons (30-100 keV) have been performed with an electron microscope column as a source of the electrons to be accelerated. The proof-of-concept experiments with sub-relativistic [24] and relativistic [23] electrons demonstrated that the maximum energy gain per single interaction can be of the order of 0.1-100 keV depending on the initial electron energy. The maximum values of acceleration gradient (energy gain per unit of propagation distance) obtained in the first experiments were  $g=25$  MeV/m [24] and  $g=300$  MeV/m [23], respectively.

To increase the efficiency of the acceleration process we extended the interaction distance and increased the coupling efficiency of the driving light to the accelerating near-field mode. These two goals were reached by modifying several experimental parameters. First significant change was the shift of the central wavelength of the driving femtosecond laser pulses from 800 nm which was used in the proof-of-concept experiments (typical wavelength for Ti:sapphire lasers) to the mid-infrared spectral region around 2000 nm (thulium or holmium-doped fiber lasers). The change of the central wavelength of the driving field was motivated by two reasons. The first is the decay length of the optical near-fields, which scales linearly with the wavelength. By increasing the wavelength 2.5-times, the decay length of the synchronous near-field for 30 keV electrons changed from 40 nm to approx. 100 nm, which relaxes the requirements for the transverse dimensions and divergence angle of the electron beam used in the experiments. The second important technological reason is that in the case of mid-infrared light, also semiconductors with high refractive index such as silicon can be used for fabrication of the periodic nanostructures used for the optical near-field generation. These high-index materials enhance the efficiency of coupling of the incident light to the synchronous evanescent field. This is not possible with the central wavelength of 800 nm, which corresponds to photon energy of 1.55 eV and is therefore strongly absorbed in semiconductor materials with band gap width  $E_g < 1.55$  eV. Due to the linear absorption, the threshold light intensity of laser-induced damage decreases significantly for 800 nm light in silicon [80].

To drive the photonic accelerators, femtosecond pulses with high amplitude of electric field are required. However, there had been no femtosecond laser oscillators or amplifiers available in the spectral region around 2  $\mu\text{m}$  until recently, when the active media based on thulium or holmium-doped glasses have been developed [81,82]. These active media can be directly pumped by laser diodes and can be prepared in a form of an optical fiber, which brings advantages such as compactness and robustness of the oscillator and amplifier designs. Fiber lasers based on these two materials have typical pulse durations of  $\tau > 500$  fs and their peak pulse energy can be scaled up to several tens of  $\mu\text{J}$  while maintaining high repetition rate of the lasers of  $f_{\text{rep}} \geq 1$  MHz. This makes these sources ideal for generating the optical near-fields for electron acceleration experiments.

Our experiments focused on different aspects of the interaction between electrons and optical fields were performed in two distinct experimental setups. The first setup, which is shown schematically in Fig. 8, is described in detail in [83]. The core of the setup was developed by Dr. J. Breuer, a former PhD student of P. Hommelhoff, and it served for the proof-of-concept experiments with sub-relativistic electrons [24,83]. During my postdoctoral fellowship, the setup was reconstructed and we added features allowing to study the spatial distribution of the electrons after the interaction with optical fields and to perform time-resolved experiments. The setup uses a DC electron beam with the maximum kinetic energy of the electrons of 30 keV, which is generated in a thermoemission electron gun of a scanning electron microscope column (Hitachi S-570). The beam is focused close to the surface of the nanostructure, which is placed in a ultrahigh vacuum (UHV) chamber on a 5D stage allowing to control the spatial overlap of the optical near-fields with the electron beam with precision of several nanometers. The near-fields are excited in a geometry, in which the laser beam is focused to the surface of the nanostructure perpendicular to the electron propagation direction. The transmitted laser light is imaged on a CCD camera (two-photon absorption of 2  $\mu\text{m}$  femtosecond pulses is used) by a combination of microscope objective and focusing lens. The spatial alignment of the overlap between electron beam and optical near-fields is performed by identifying the position of both beams at the surface of the nanostructure in both the optical and electron microscope images.

After the interaction with optical fields, the electron spectrum is characterized using a retarding-field spectrometer [84], which serves as a high pass filter for the electrons, and a microchannel plate (MCP) detector. The energy resolution of the setup is  $\approx 10$  eV at the electron energy of 30 keV. To obtain the full spectrum we change the retardation voltage applied to the spectrometer and measure the transmitted electron current. The signal from X-rays generated in the microscope column is filtered out by using a coil to bend the electron beam in front of the detector. X-ray radiation is blocked using a metallic sheet.

Because the optical near-fields at the nanostructure are excited using a femtosecond laser (in this case it is an experimental fiber oscillator+amplifier system from Menlo Lasers based on thulium-doped fiber, pulse duration  $\tau=500$  fs, pulse energy up to 1  $\mu\text{J}$ , repetition rate 1 MHz) with the duty cycle of only  $10^{-7}$ , only a small fraction of the electrons from the DC electron beam could interact with the optical near-fields. To detect these electrons, the time-resolved electronic signal from the MCP is measured and correlated to the signal from a fast photodiode (avalanche photodiode), which detects the arrival time of each laser pulse. The two electronic signals are processed by a time-to-digital converter (TDC), which measures the time delay between the start signal obtained from the MCP and the signal from the subsequent laser pulse generated at the avalanche photodiode. The measured time delays are plotted as a histogram showing the number of detected above-threshold events per unit of the time delay. The interacting electrons form a peak, which is surrounded by the background caused by the signal from dark current of the MCP and the electrons scattered in the vacuum chamber, which can eventually reach the MCP. The experiments were performed under UHV conditions at pressures below  $10^{-6}$  mbar.

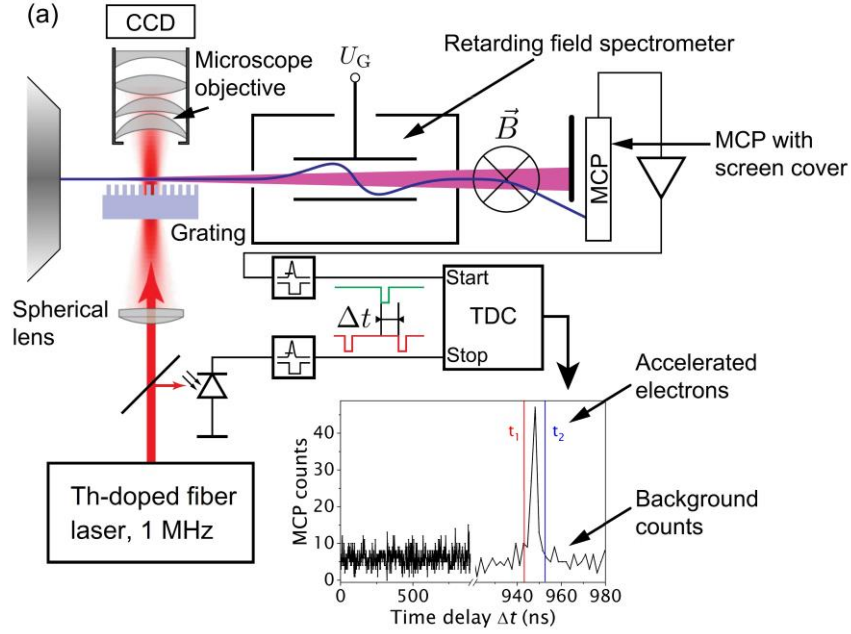


Fig. 8. The layout of the experimental setup used for investigation of the interaction between free electrons and optical near-fields of nanostructures (adapted from [83]). Electron beam (blue) propagating from left to the right is focused to the interaction region close to the surface of a dielectric grating, which is illuminated by the femtosecond laser beam (red). After the interaction, the electrons propagate through a retarding-field spectrometer to the MCP detector. Time-resolved electronic signal from MCP is used as a start signal for TDC unit, which measures the time delay of the subsequent laser pulse and plot the individual events to the histogram (bottom right), which shows a background and a single peak corresponding to accelerated electrons.

The second experimental setup (see Fig. 9a)) was developed by me during my postdoctoral research fellowship at FAU Erlangen-Nürnberg in the group of P. Hommelhoff. The electron source is based on a laser-triggered scanning electron microscope column with Schottky-type electron source [85] (FEI XL 30 FEG), which produces femtosecond electron pulses that can be focused by electron optics to spot sizes of several nanometers. The electron emission timing is controlled by ultraviolet femtosecond laser pulses with duration of  $\approx 100$  fs focused to the surface of the tungsten tip, which in classical DC operation of the microscope serves for field-emission of electrons in the gun. When the surface is illuminated by photons with photon energy  $\hbar\omega \geq W$ , where  $W$  is the work function of the surface, the electrons are emitted via photoeffect. The work function is reduced by  $ZrO_x$  deposited to the tip surface from the reservoir placed at the heated supporting wire and also by the applied electric field between the tip and extractor anode [85].

When the tip temperature decreases below a certain value, the electric field at the tip surface is below the field emission threshold and no DC electron emission occurs. However, when the tip is heated to a high temperature by electric current sent through a supporting wire, the DC field emission becomes possible. This offers a convenient mechanism allowing to switch between the laser-driven pulsed photoemission regime with lower heating of the tip and a standard continuous electron beam, which is used for imaging of the structures and during alignment of the experiments. Controlling the time envelope of the electron pulses allows us to reach a regime, in which almost all

the electrons interact with the optical fields generated by the same pulsed laser which triggers the electron emission.

The electron spectrum after the interaction is characterized using a single prism Elbek-type magnetic spectrometer [86] and an MCP detector. The spatially resolved images from the MCP allow to characterize the full electron spectrum in one measurement while for the previous setup it was necessary to scan the voltage applied to the retarding-field spectrometer to measure the electron energy spectra. The properties and performance of the laser-triggered SEM are discussed in detail in [A11]. Here I only mention the shortest measured electron pulse duration of  $\tau=460$  fs (FWHM) in the regime of less than 1 electron per pulse on average emitted from the tip. We typically used this regime for the presented measurements because the electron pulse duration and spot size in focus are not influenced by Coulomb repulsion, which occurs for multielectron pulses in short times after emission from the tip [64,65].

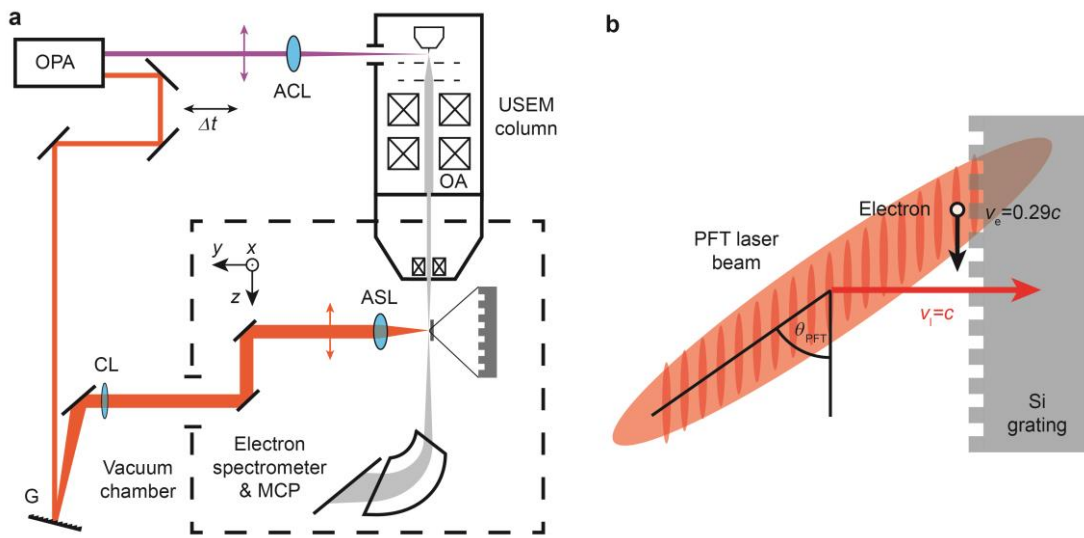


Fig. 9. a) Layout of the ultrafast scanning electron microscope (USEM) experimental setup [A11]. The pulsed UV laser beam (violet) generated in an optical parametric amplifier (OPA) is focused by an achromatic lens (ACL) to the USEM Schottky tip, where the electrons are photoemitted. The pulsed electron beam (grey) is transmitted through the objective aperture (OA) and is focused to the interaction region to the vicinity of the surface of a periodic dielectric nanostructure. The pulsed IR laser beam (red), which is used for optical near-field generation, is delayed by an optical delay line ( $\Delta t$ ) and dispersed by a diffraction grating (G), whose surface is imaged by a cylindrical lens (CL) and an aspherical lens (ASL) to the surface of the nanostructure in the USEM vacuum chamber. Electron spectra are measured by an electromagnetic spectrometer and a micro-channel plate detector (MCP). b) Interaction between an electron propagating downwards along the surface of a silicon grating and optical near-fields generated by a pulse-front-tilted laser beam propagating horizontally from the left to the right.

To extend the effective interaction distance/time we introduced a pulse-front tilt [87] to the infrared laser pulses generating the optical near-fields. In the pulse-front-tilted state, the surfaces of constant phase and constant intensity of the optical pulses are not parallel (see Fig. 9b)). The group velocity of the envelope of the synchronous near-field in the direction of electron propagation is matched to its phase velocity. This is reached by imaging the surface of the reflective diffraction grating

(element G in Fig. 9a)) using a cylindrical and spherical lenses. By adjusting the angular dispersion of the grating and focal distances of the imaging setup it is possible to control the pulse-front tilt angle  $\theta_{\text{PFT}}$ .

The same experimental setup was also used to study the inelastic electron interaction with ponderomotive potential of optical travelling waves [A7,A8]. Here the optical part was modified. By using two optical beam paths and two independent focusing lenses we intersected the two laser pulses at different frequencies with the pulsed electron beam (details can be found in ref. [A7] and its Supplementary Information).

Besides the experiments demonstrating the photon-electron interaction, the pulsed electron microscope setup can serve also for time-resolved experiments, in which a laser pulse is used to excite dynamics in the studied sample and an electron pulse serves as a probe and image the dynamics after the optical excitation with high spatial resolution [2]. The time-resolved experiments with single-electron pulses are then typically performed in a stroboscopic manner, in which many subsequent measurements are done with the same time delay between the electron and laser pulses to allow image formation. This process is repeated for different time delays and allows to monitor the dynamical changes induced in the sample. Such stroboscopic imaging has one important pre-requisite. The studied sample has to get back to the initial state before the next excitation pulse comes. Ultrafast scanning electron microscopy was applied e.g. to study the excited carrier dynamics in a p-n junction [88] or to image diffusing carriers in semiconductors [89].

### 3.2. Overview of the results

The experimental setups described in the previous section served for various experiments focused on the research of the inelastic electron interaction with light fields. Besides the experiments, several publications attached to this thesis are focused on theory and numerical simulations. The publications can be divided to two categories according to the type of the interaction which is investigated.

In the first category we studied electron scattering at optical near-fields with several goals:

- 1) Enhancement of the coupling efficiency of light to the synchronous mode by using different light wavelengths, optimized nanostructures fabricated from high-index and high damage-threshold materials, development of new type of enhancement based on distributed Bragg mirrors [A12,A14]
- 2) Demonstration of the sub-cycle structure of electron energy modulation [A4]
- 3) Acceleration of the electrons to the highest possible energies [A9,A11]
- 4) Demonstration of new types of coupling of incident light waves to evanescent synchronous modes [A5]
- 5) Studies of various aspects of electron acceleration by optical near-fields [A2,A3,A6,A9,A11]

The goals were motivated by the proof-of-concept experiments [23,24], which showed only the basic properties of the interaction. This type of experiments is nontrivial as it combines several distinct areas of physics, namely femtosecond laser optics, electron emission physics and optics and nanofabrication, which is required to obtain the nanostructures for generation of the optical near-fields. The structures were fabricated using standard nanofabrication techniques. First the design of each structure

was optimized using FDTD simulations and then it was patterned in a photoresist, which was deposited to a flat surface of a crystalline substrate (most often silicon). For patterning we used electron beam lithography or UV lithography for larger details of the structures. After this step, the illuminated resist was washed away and the structure was etched using reactive ion etching. The nanofabrication for most of the publications included in this thesis [A3,A4,A5,A6,A9,A11] was performed by our collaborators at Stanford University (groups of prof. Harris and prof. Byer). The same nanofabrication process was also used by our colleague P. Yousefi at Max-Planck Institute in Erlangen, where the structures with distributed Bragg reflectors were prepared [A12].

To enhance the efficiency of light coupling to the synchronous optical mode we adapted the optical part of the experimental setup for light at mid-infrared driving wavelengths of about 2 micrometers. This allowed us to use silicon nanostructures with two advantages compared to SiO<sub>2</sub> structures used for the initial experiments. First advantage is the technology of nanofabrication, which is well developed for silicon and enables precise fabrication of complex structures with various shapes with few-nanometer spatial resolution. Second advantage is very large refractive index of silicon of  $n=3.4$ , which helps to increase the coupling of light to slow evanescent modes significantly. In the publication [A12] we developed a new type of periodic structure, which uses rows of nanopillars to generate the synchronous optical near-field instead of rectangular grating. This structure was inspired by our colleagues at Stanford University [90]. To enhance the coupling efficiency even more and to generate almost symmetric transverse field profile we added two features, namely the spatial offset of the pillars and the Bragg reflector, which emulates the illumination of the structure from opposite direction. As we showed in [A12], such Bragg reflector increases the efficiency of synchronous mode excitation approximately by 60%.

Next goal was to demonstrate the harmonic energy modulation of the electrons after the interaction with optical near-fields. If the concept of time-to-energy mapping can be transferred to free electrons, it would enable streaking-based metrology and control of electron beams on attosecond time scales [A4]. To study the sub-cycle modulation we let the electrons interact with two subsequent synchronous waves, which were phase-locked to each other. These two waves were generated in a Michelson interferometer and focused to two spatially separated spots on a single silicon grating. By changing the relative phase between the two optical waves with which the electrons interacted we were able to modulate the final energy spectrum [A4]. When the two waves act in phase, the spectral modulation is enhanced while the out of phase operation leads to suppression of the energy modulation. We also showed for the first time that the optical near-fields can cause transverse streaking of the electrons depending on their arrival time with respect to the optical wave [A4]. The numerical simulations show a possibility to reach time resolution of about 10 attoseconds in transverse streaking-based characterization of electron pulses.

One of the motivations of our research was to construct a light-driven electron accelerator based on synchronous optical near-fields. However, with increasing energy gain of slow electrons (kinetic energy of 1-30 keV), the propagation velocity of the electrons changes significantly and it is no longer synchronous to the optical near-field mode. A solution of this problem is to create an accelerating evanescent wave with the propagation velocity changing along the electron beam path. Two possibilities how to generate such accelerating wave are to use chirped laser pulses to drive the interaction or to create a chirped quasiperiodic structure, at which the spatial period changes along the electron propagation direction. We chose the second possibility for practical reasons. Chirping the laser pulses would require broadband laser source and a more

complex optical setup while chirping the nanostructure can be easily reached by modifying the structure design. Such chirped structures allowed us to increase the maximum energy gain of electrons with the initial kinetic energy of 28 keV to  $\Delta E_k=2.6$  keV (almost 10% relative change of the electron energy, which is still highest value of the relative energy gain for this type of electron acceleration) [A9]. Besides the acceleration, the electrons in any accelerator structure have to be guided by transverse forces to allow the acceleration to high energies over extended distances. As I discuss in chapter 2.2, the phase-shifted transverse forces are naturally present during the interaction with optical near-fields. In [A9] we showed that by special design of the nanostructures, the transverse forces can be controlled to some extent and can guide or focus the electron beam.

To further explore different possibilities of light coupling to the synchronous near-field we studied a case, in which no nanostructure is required. The evanescent optical waves appear already in basic courses of wave optics during a phenomenon of total internal reflection. When the angle of incidence of a light wave propagating through a planar boundary between higher and lower refractive index materials is higher than the critical angle, the light wave becomes totally reflected [91]. This effect is accompanied by generation of an evanescent wave, which propagates along the boundary in the lower-index material. When the first material is a dielectric and the second material is vacuum, the electrons can propagate along the boundary on the vacuum side and synchronously interact with the evanescent wave. We introduced and studied this coupling mechanism both theoretically and experimentally [A5]. It has already found interesting applications for pulsed [10,92] or continuous [77,78] electron phase modulation in transmission electron microscopes or in advanced schemes for photonic electron accelerators [93].

Further we investigated various other aspects of the electron-light interaction, such as the possibility to drive the interaction with extremely short laser pulses [A6] or the possibility to use the optical near-fields as a beam position and timing monitor with high spatial and temporal resolutions [A3].

In the second category of papers we investigated both theoretically and experimentally the interaction of electrons with the ponderomotive potential of optical fields in vacuum. We performed proof-of-principle experiments demonstrating the inelastic electron scattering at the ponderomotive potential of an optical travelling wave [A7] and generation and detection of attosecond electron pulses by this technique [A8]. We showed that using the ponderomotive potential it is possible to reach an effective field of 2.5 GV/m and accelerate the electrons from initial kinetic energy of 30 keV by more than 10 keV. When taking into account the photon energy of the driving photons of about 0.5 eV, this corresponds to absorption and simultaneous emission of more than 10.000 photons by the electron during the interaction time of only  $\approx 50$  fs.

As described in chapters 2.3. and 2.4., the harmonic energy modulation of the electrons leads to a formation of attosecond-long spikes in the electron probability distribution. In [A8] we investigated this type of electron compression and showed that it is possible to control the dynamics of the electrons in the longitudinal phase space using the strength of the interaction with optical fields. We created two phase-locked spatially separated interaction regions. The arrival time of the electron pulse train with respect to the second streaking wave depends on the relative phase difference. From the measured spectrograms (electron spectra as a function of the relative phase difference between the two optical waves) we were able to identify the conditions for optimal electron compression. By comparing the experimental results with numerical



simulations, the duration of individual electron pulses from the train were determined to be  $\approx 300$  attoseconds [A8]. The paper also shows that it is possible to reach long-term stability, which is sufficient for performing imaging experiments with compressed electrons with sub-femtosecond time resolution.

Besides the experimental studies I investigated several novel aspects of the electron-light interaction in vacuum. Using numerical simulations I described how the chirped laser pulses can serve for efficient electron acceleration from rest to high energies [A1]. Further I studied the possibility to generate isolated attosecond electron pulses using the interaction with three pulsed laser beams [A13] and proposed generation of electron vortex states via inelastic scattering at optical ponderomotive potential [A15]. Finally I theoretically studied higher-order nonlinear inelastic scattering of electrons at optical standing waves [A10].

The real applications of the phenomena introduced and studied in the collection of papers of this thesis require as high current of electrons as possible. However, to reach high enough strength of the interaction with optical fields, the driving optical waves have to be pulsed with very short pulse durations of the order of hundreds of femtoseconds to picoseconds. The limitation for practical applicability thus arises from the fact that the electrons are fermions that carry charge. The maximum current density and peak brightness of an electron beam is limited by Coulomb interactions between the electrons [64,65]. For the experiments with optical near-fields, the beam has to be compressed in all three dimensions due to a sharp spatial decay of the evanescent wave amplitude. It can be shown that it is not possible to propagate high density of sub-relativistic electrons in a bunch with nanometric dimensions over extended distances. For this reason, most of the experiments have to be done in a repetitive manner with high repetition rate femtosecond laser systems, which allow to increase the average current of electrons interacting with the optical fields to picoampere level. This is already enough for formation of real of diffraction images within reasonable acquisition time of few seconds.

Further details of all the performed experiments, theory and numerical modelling can be found in the papers attached to this thesis and their supplementary materials.

## 4. Conclusion & outlook

The research presented in this thesis is focused on different aspects of stimulated inelastic interactions between electrons freely propagating in vacuum and light fields. We proposed and demonstrated several important advancements in this research field. The most important finding and experimental achievement is the possibility to control the electrons by the electromagnetic fields of light waves on sub-femtosecond time scales, which were not reached previously. The possible applications of electron beams compressed to attosecond durations span from phase-resolved imaging of optical and plasmonic near-fields to the control of electron injection to laser-driven electron accelerators. However, there are also interesting quantum mechanical aspects of the interaction, which we plan to study in the near future.

As discussed in chapter 2, the electron wavepacket interacting with synchronous optical field obtains a phase modulation at the optical frequency. An unresolved question of fundamental importance is whether the optical coherence imprinted to a single electron wavepacket by a coherent light wave can be transferred to other types of electronic excitations and/or to photons generated via cathodoluminescence (Smith-Purcell [94], coherent transition radiation [95] or other types of coherent emission processes). This question is related to a long-lasting controversy between the two possible interpretations of a free massive particle and its interactions. The first interpretation consider the square modulus of the wavefunction as the probability distribution of finding a point-like particle in a particular state (position, momentum) [96] while the second interpretation connects it with the continuous charge density represented by a spreading wavepacket. The difference has implications for the radiation emitted by the electrons while propagating in periodic fields [97], close to refractive materials [69] or for the possible resonant interaction with two-level quantum systems [12]. The transfer of coherence has been theoretically considered only recently, but it has never been observed. Combined with the atomic resolution of electron microscopes, such process would enable to address and coherently control quantum states of a single atom in an ensemble (solids state material, molecule, etc.) or to coherently drive photon emission from a selected two-level system, thus going significantly beyond the state of the art in the field of quantum control and metrology. Besides low-energy excitations and photon emission, the attosecond time structure of the electron wavepackets may be applied in future for time-resolved studies of correlated inner-shell electron dynamics such as Auger decay in atoms, which typically occurs on single femtosecond time scales [98].

Another possible application of quantum coherent optically modulated electron waves is a new type of electron holography, in which the electron waves are shifted in the time domain (along the beam propagation direction). The first interaction would serve as a coherent beamsplitter and the momentum shifted electron states would interfere in a second interaction with the optical near-fields of the sample to be studied. This type of time domain electron holography may enable phase-resolved imaging of optical and plasmonic near-fields and to study their generation and propagation with unprecedented combination of attosecond temporal and nanometer spatial resolutions. With this being said, this research field provides a lot of different directions for future research and many new avenues to be explored in next few years.

## Bibliography

- [1] Y. Jiang, Z. Chen, Y. Han, P. Deb, H. Gao, S. Xie, P. Purohit, M. W. Tate, J. Park, S. M. Gruner, V. Elser, and D. A. Muller, *Electron Ptychography of 2D Materials to Deep Sub-Ångström Resolution*, *Nature* **559**, 343 (2018).
- [2] D. J. Flannigan and A. H. Zewail, *4D Electron Microscopy: Principles and Applications*, *Accounts of Chemical Research* **45**, 1828 (2012).
- [3] H. Ihee, V. A. Lobastov, U. M. Gomez, B. M. Goodson, R. Srinivasan, C. Y. Ruan, and A. H. Zewail, *Direct Imaging of Transient Molecular Structures with Ultrafast Diffraction*, *Science* **291**, 458 (2001).
- [4] B. J. Siwick, J. R. Dwyer, R. E. Jordan, and R. J. D. Miller, *An Atomic-Level View of Melting Using Femtosecond Electron Diffraction*, *Science* **302**, 1382 (2003).
- [5] M. Möller, J. H. Gaida, S. Schäfer, and C. Ropers, *Few-Nm Tracking of Current-Driven Magnetic Vortex Orbits Using Ultrafast Lorentz Microscopy*, *Communications Physics* **3**, 36 (2020).
- [6] P. Baum, *On the Physics of Ultrashort Single-Electron Pulses for Time-Resolved Microscopy and Diffraction*, *Chemical Physics* **423**, 55 (2013).
- [7] A. Feist, K. E. Echternkamp, J. Schauss, S. v. Yalunin, S. Schäfer, and C. Ropers, *Quantum Coherent Optical Phase Modulation in an Ultrafast Transmission Electron Microscope*, *Nature* **521**, 200 (2015).
- [8] A. Feist, S. V Yalunin, S. Schäfer, and C. Ropers, *High-Purity Free-Electron Momentum States Prepared by Three-Dimensional Optical Phase Modulation*, *Phys. Rev. Research* **2**, 43227 (2020).
- [9] K. E. Echternkamp, A. Feist, S. Schäfer, and C. Ropers, *Ramsey-Type Phase Control of Free-Electron Beams*, *Nature Physics* **12**, 1000 (2016).
- [10] O. Kfir, H. Lourenço-Martins, G. Storeck, M. Sivi, T. R. Harvey, T. J. Kippenberg, A. Feist, and C. Ropers, *Controlling Free Electrons with Optical Whispering-Gallery Modes*, *Nature* **582**, 46 (2020).
- [11] P. Baum, *Quantum Dynamics of Attosecond Electron Pulse Compression*, *Journal of Applied Physics* **122**, 223105 (2017).
- [12] A. Gover and A. Yariv, *Free-Electron–Bound-Electron Resonant Interaction*, *Physical Review Letters* **124**, 064801 (2020).
- [13] O. Reinhardt, C. Mechel, M. Lynch, and I. Kaminer, *Free-Electron Qubits*, *Annalen Der Physik* **533**, 2000254 (2021).
- [14] O. Reinhardt and I. Kaminer, *Theory of Shaping Electron Wavepackets with Light*, *ACS Photonics* **7**, 2859 (2020).
- [15] F. J. de Abajo and A. Konečná, *Optical Modulation of Electron Beams in Free Space*, *Phys. Rev. Lett.* **126**, 123901 (2021).
- [16] C. Pellegrini, A. Marinelli, and S. Reiche, *The Physics of X-Ray Free-Electron Lasers*, *Reviews of Modern Physics* **88**, 15006 (2016).
- [17] E. Prat, R. Abela, M. Aiba, A. Alarcon, J. Alex, Y. Arbelo, C. Arrell, V. Arsov, C. Bacellar, C. Beard, P. Beaud, S. Bettoni, R. Biffiger, M. Bopp, H.-H. Braun, M. Calvi, A. Cassar, T. Celcer, M. Chergui, P. Chevtsov, C. Cirelli, A. Citterio, P. Craievich, M. C. Divall, A. Dax, M. Dehler, Y. Deng, A. Dietrich, P. Dijkstal, R. Dinapoli, S. Dordevic, S. Ebner, D. Engeler, C. Erny, V. Esposito, E. Ferrari, U. Flechsig, R. Follath, F. Frei, R. Ganter, T. Garvey, Z. Geng, A. Gobbo, C. Gough, A. Hauff, C. P. Hauri, N. Hiller, S. Hunziker, M. Huppert, G. Ingold, R. Ischebeck, M. Janousch, P. J. M. Johnson, S. L. Johnson, P. Juranić, M. Jurcevic, M. Kaiser, R. Kalt, B. Keil, D. Kiselev, C.

- Kittel, G. Knopp, W. Koprek, M. Laznovsky, H. T. Lemke, D. L. Sancho, F. Löh, A. Malyzhenkov, G. F. Mancini, R. Mankowsky, F. Marcellini, G. Marinkovic, I. Martiel, F. Märki, C. J. Milne, A. Mozzanica, K. Nass, G. L. Orlandi, C. O. Loch, M. Paraliiev, B. Patterson, L. Patthey, B. Pedrini, M. Pedrozzi, C. Pradervand, P. Radi, J.-Y. Raguin, S. Redford, J. Rehanek, S. Reiche, L. Rivkin, A. Romann, L. Sala, M. Sander, T. Schietinger, T. Schilcher, V. Schlott, T. Schmidt, M. Seidel, M. Stadler, L. Stingelin, C. Svetina, D. M. Treyer, A. Trisorio, C. Vicario, D. Voulot, A. Wrulich, S. Zerdane, and E. Zimoch, *A Compact and Cost-Effective Hard X-Ray Free-Electron Laser Driven by a High-Brightness and Low-Energy Electron Beam*, *Nature Photonics* **14**, 748 (2020).
- [18] T. Tajima and J. M. Dawson, *Laser Electron Accelerator*, *Physical Review Letters* **43**, 267 (1979).
- [19] G. K. S. J. L. C. Gérard A. Mourou, editor, *WHITEBOOK ELI – Extreme Light Infrastructure; Science and Technology with Ultra-Intense Lasers* (Andreas Thoss, 2011).
- [20] L. Lilje, E. Kako, D. Kostin, A. Matheisen, W.-D. Möller, D. Proch, D. Reschke, K. Saito, P. Schmüser, S. Simrock, T. Suzuki, and K. Twarowski, *Achievement of 35MV/m in the Superconducting Nine-Cell Cavities for TESLA*, *Nuclear Instruments and Methods in Physics Research Section A: Accelerators, Spectrometers, Detectors and Associated Equipment* **524**, 1 (2004).
- [21] K. Shimoda, *Proposal for an Electron Accelerator Using an Optical Maser*, *Appl. Opt.* **1**, 33 (1962).
- [22] Y. Takeda and I. Matsui, *Laser Linac with Grating*, *Nuclear Instruments and Methods* **62**, 306 (1968).
- [23] E. A. Peralta, K. Soong, R. J. England, E. R. Colby, Z. Wu, B. Montazeri, C. McGuinness, J. McNeur, K. J. Leedle, D. Walz, E. B. Sozer, B. Cowan, B. Schwartz, G. Travish, and R. L. Byer, *Demonstration of Electron Acceleration in a Laser-Driven Dielectric Microstructure*, *Nature* **503**, 91 (2013).
- [24] J. Breuer and P. Hommelhoff, *Laser-Based Acceleration of Nonrelativistic Electrons at a Dielectric Structure*, *Physical Review Letters* **111**, 134803 (2013).
- [25] J. Breuer, J. McNeur, and P. Hommelhoff, *Dielectric Laser Acceleration of Electrons in the Vicinity of Single and Double Grating Structures - Theory and Simulations*, *Journal of Physics B: Atomic, Molecular and Optical Physics* **47**, 234004 (2014).
- [26] N. Schönenberger, A. Mittelbach, P. Yousefi, J. McNeur, U. Niedermayer, and P. Hommelhoff, *Generation and Characterization of Attosecond Microbunched Electron Pulse Trains via Dielectric Laser Acceleration*, *Phys. Rev. Lett.* **123**, 264803 (2019).
- [27] K. E. Priebe, C. Rathje, S. V. Yalunin, T. Hohage, A. Feist, S. Schäfer, and C. Ropers, *Attosecond Electron Pulse Trains and Quantum State Reconstruction in Ultrafast Transmission Electron Microscopy*, *Nature Photonics* **11**, 793 (2017).
- [28] Y. Morimoto and P. Baum, *Diffraction and Microscopy with Attosecond Electron Pulse Trains*, *Nature Physics* **14**, 252 (2018).
- [29] G. M. Vanacore, I. Madan, G. Berruto, K. Wang, E. Pomarico, R. J. Lamb, D. McGrouther, I. Kaminer, B. Barwick, F. J. García De Abajo, and F. Carbone,

- Attosecond Coherent Control of Free-Electron Wave Functions Using Semi-Infinite Light Fields*, Nature Communications **9**, 2694 (2018).
- [30] S. Yu. Kruchinin, F. Krausz, and V. S. Yakovlev, *Colloquium: Strong-Field Phenomena in Periodic Systems*, Rev. Mod. Phys. **90**, 21002 (2018).
- [31] D. J. Jones, S. A. Diddams, J. K. Ranka, A. Stentz, R. S. Windeler, J. L. Hall, and S. T. Cundiff, *Carrier-Envelope Phase Control of Femtosecond Mode-Locked Lasers and Direct Optical Frequency Synthesis*, Science **288**, 635 (2000).
- [32] F. Krausz and M. Ivanov, *Attosecond Physics*, Reviews of Modern Physics **81**, 163 (2009).
- [33] M. Drescher, M. Hentschel, R. Kienberger, M. Uiberacker, V. Yakovlev, A. Scrinzi, T. Westerwalbesloh, U. Kleineberg, U. Heinzmann, and F. Krausz, *Time-Resolved Atomic Inner-Shell Spectroscopy*, Nature **419**, 803 (2002).
- [34] M. Meckel, D. Comtois, D. Zeidler, A. Staudte, D. Pavičić, H. C. Bandulet, H. Pépin, J. C. Kieffer, R. Dörner, D. M. Villeneuve, and P. B. Corkum, *Laser-Induced Electron Tunneling and Diffraction*, Science **320**, 1478 (2008).
- [35] H. Lakhota, H. Y. Kim, M. Zhan, S. Hu, S. Meng, and E. Goulielmakis, *Laser Picoscopy of Valence Electrons in Solids*, Nature **583**, 55 (2020).
- [36] A. Schiffrin, T. Paasch-Colberg, N. Karpowicz, V. Apalkov, D. Gerster, S. Mühlbrandt, M. Korbman, J. Reichert, M. Schultze, S. Holzner, J. V Barth, R. Kienberger, R. Ernstorfer, V. S. Yakovlev, M. I. Stockman, and F. Krausz, *Optical-Field-Induced Current in Dielectrics*, Nature **493**, 70 (2013).
- [37] M. Lucchini, S. A. Sato, A. Ludwig, J. Herrmann, M. Volkov, L. Kasmi, Y. Shinohara, K. Yabana, L. Gallmann, and U. Keller, *Attosecond Dynamical Franz-Keldysh Effect in Polycrystalline Diamond*, Science **353**, 916 (2016).
- [38] E. Goulielmakis, M. Uiberacker, R. Kienberger, A. Baltuska, V. Yakovlev, A. Scrinzi, Th. Westerwalbesloh, U. Kleineberg, U. Heinzmann, M. Drescher, and F. Krausz, *Direct Measurement of Light Waves*, Science **305**, 1267 (2004).
- [39] E. Goulielmakis, Z.-H. Loh, A. Wirth, R. Santra, N. Rohringer, V. S. Yakovlev, S. Zherebtsov, T. Pfeifer, A. M. Azzeer, M. F. Kling, S. R. Leone, and F. Krausz, *Real-Time Observation of Valence Electron Motion*, Nature **466**, 739 (2010).
- [40] M. Kozák, T. Otobe, M. Zukerstein, F. Trojánek, and P. Malý, *Anisotropy and Polarization Dependence of Multiphoton Charge Carrier Generation Rate in Diamond*, Phys. Rev. B **99**, 104305 (2019).
- [41] M. Zukerstein, F. Trojánek, B. Rezek, Z. Šobán, M. Kozák, and P. Malý, *Coherent Phonon Dynamics in Diamond Detected via Multiphoton Absorption*, Applied Physics Letters **115**, 161104 (2019).
- [42] M. Kozák, P. Peterka, J. Dostál, F. Trojánek, and P. Malý, *Generation of Few-Cycle Laser Pulses at 2 Mm with Passively Stabilized Carrier-Envelope Phase Characterized by  $f$ - $3f$  Interferometry*, Optics & Laser Technology **144**, 107394 (2021).
- [43] J. D. Lawson, *Lasers and Accelerators*, IEEE Transactions on Nuclear Science **26**, 4217 (1979).
- [44] R. B. Palmer, *An Introduction to Acceleration Mechanisms*, (SLAC-PUB--4320) United States, 1987.
- [45] H. A. H. Boot and R. B. R.-S.-Harvie, *Charged Particles in a Non-Uniform Radio-Frequency Field*, Nature **180**, 1187 (1957).

- [46] P. L. Kapitza and P. A. M. Dirac, *The Reflection of Electrons from Standing Light Waves*, Mathematical Proceedings of the Cambridge Philosophical Society **29**, 297 (1933).
- [47] P. L. Gould, G. A. Ruff, and D. E. Pritchard, *Diffraction of Atoms by Light: The near-Resonant Kapitza-Dirac Effect*, Phys. Rev. Lett. **56**, 827 (1986).
- [48] D. L. Freimund, K. Aflatooni, and H. Batelaan, *Observation of the Kapitza-Dirac Effect*, Nature **413**, 142 (2001).
- [49] H. Batelaan, *Colloquium: Illuminating the Kapitza-Dirac Effect with Electron Matter Optics*, Reviews of Modern Physics **79**, 929 (2007).
- [50] P. H. Bucksbaum, D. W. Schumacher, and M. Bashkansky, *High-Intensity Kapitza-Dirac Effect*, Physical Review Letters **61**, 1182 (1988).
- [51] M. A. Efremov and M. v Fedorov, *Classical and Quantum Versions of the Kapitza-Dirac Effect*, Journal of Experimental and Theoretical Physics **89**, 460 (1999).
- [52] V. M. Haroutunian and H. K. Avetissian, *An Analogue of the Kapitza-Dirac Effect*, Physics Letters A **51**, 320 (1975).
- [53] P. Baum and A. H. Zewail, *Attosecond Electron Pulses for 4D Diffraction and Microscopy*, Proceedings of the National Academy of Sciences of the United States of America **104**, 18409 (2007).
- [54] A. H. Compton, *A Quantum Theory of the Scattering of X-Rays by Light Elements*, Physical Review **21**, 483 (1923).
- [55] O. Klein and Y. Nishina, *Über Die Streuung von Strahlung Durch Freie Elektronen Nach Der Neuen Relativistischen Quantendynamik von Dirac*, Zeitschrift Für Physik **52**, 853 (1929).
- [56] S. T. Park, M. Lin, and A. H. Zewail, *Photon-Induced near-Field Electron Microscopy (PINEM): Theoretical and Experimental*, New Journal of Physics **12**, 123028 (2010).
- [57] F. J. García De Abajo, *Optical Excitations in Electron Microscopy*, Reviews of Modern Physics **82**, 209 (2010).
- [58] F. J. García de Abajo and V. di Giulio, *Optical Excitations with Electron Beams: Challenges and Opportunities*, ACS Photonics **8**, 945 (2021).
- [59] F. J. Garcia De Abajo, A. Asenjo-Garcia, and M. Kociak, *Multiphoton Absorption and Emission by Interaction of Swift Electrons with Evanescent Light Fields*, Nano Letters **10**, 1859 (2010).
- [60] N. Ida, *Numerical Modeling for Electromagnetic Non-Destructive Evaluation*. (Chapman & Hall., London, 1995).
- [61] T. Weiland, *Time domain electromagnetic field computation with finite difference methods*, International Journal of Numerical Modelling: Electronic Networks, Devices and Fields **9**, 295 (1996).
- [62] K. Yee, *Numerical Solution of Initial Boundary Value Problems Involving Maxwell's Equations in Isotropic Media*, IEEE Transactions on Antennas and Propagation **14**, 302 (1966).
- [63] *Lumerical FDTD*, URL: <https://www.lumerical.com/products/fdtd/>.
- [64] B. Cook and P. Kruit, *Coulomb Interactions in Sharp Tip Pulsed Photo Field Emitters*, Applied Physics Letters **109**, 151901 (2016).
- [65] B. Cook, T. Verduin, C. W. Hagen, and P. Kruit, *Brightness Limitations of Cold Field Emitters Caused by Coulomb Interactions*, Journal of Vacuum Science & Technology B **28**, C6C74 (2010).
- [66] A. Lubk, *Paraxial Quantum Mechanics*, Advances in Imaging and Electron Physics **206**, 15 (2018).

- [67] N. Talebi, *Strong Interaction of Slow Electrons with Near-Field Light Visited from First Principles*, Physical Review Letters **125**, (2020).
- [68] I. Madan, G. M. Vanacore, E. Pomarico, G. Berruto, R. J. Lamb, D. McGrouther, T. T. A. Lummen, T. Latychevskaia, F. J. García de Abajo, and F. Carbone, *Holographic Imaging of Electromagnetic Fields via Electron-Light Quantum Interference*, Science Advances **5**, eaav8358 (2019).
- [69] O. Kfir, V. di Giulio, F. J. G. de Abajo, C. Ropers, V. di Giulio, F. J. G. de Abajo, and C. Ropers, *Optical Coherence Transfer Mediated by Free Electrons*, Science Advances **7**, eabf6380 (2020).
- [70] R. L. Fork, C. H. Brito Cruz, P. C. Becker, and C. v Shank, *Compression of Optical Pulses to Six Femtoseconds by Using Cubic Phase Compensation*, Optics Letters **12**, 483 (1987).
- [71] O. E. Martinez, *Grating and Prism Compressors in the Case of Finite Beam Size*, Journal of the Optical Society of America B **3**, 929 (1986).
- [72] R. Szipöcs, K. Ferencz, C. Spielmann, and F. Krausz, *Chirped Multilayer Coatings for Broadband Dispersion Control in Femtosecond Lasers*, Optics Letters **19**, 201 (1994).
- [73] A. Gliserin, M. Walbran, F. Krausz, and P. Baum, *Sub-Phonon-Period Compression of Electron Pulses for Atomic Diffraction*, Nature Communications **6**, 8723 (2015).
- [74] C. Kealhofer, W. Schneider, D. Ehberger, A. Ryabov, F. Krausz, and P. Baum, *All-Optical Control and Metrology of Electron Pulses*, Science **352**, 429 (2016).
- [75] Y. Morimoto and P. Baum, *Attosecond Control of Electron Beams at Dielectric and Absorbing Membranes*, Physical Review A **97**, 033815 (2018).
- [76] D. Raphael, G. Alexey, H. Urs, K. Aviv, E. Ori, Y. Peyman, S. Mordechai, A. Ady, E. Gadi, H. Peter, and K. Ido, *Imprinting the Quantum Statistics of Photons on Free Electrons*, Science **373**, eabj7128 (2022).
- [77] J.-W. Henke, A. S. Raja, A. Feist, G. Huang, G. Arend, Y. Yang, F. J. Kappert, R. N. Wang, M. Möller, J. Pan, J. Liu, O. Kfir, C. Ropers, and T. J. Kippenberg, *Integrated Photonics Enables Continuous-Beam Electron Phase Modulation*, Nature **600**, 653 (2021).
- [78] M. Kozak, *Photonics Low-Power Light Modifies Electron Microscopy*, Nature **600**, 610 (2021).
- [79] K. Wang, R. Dahan, M. Shentcis, Y. Kauffmann, A. ben Hayun, O. Reinhardt, S. Tsesses, and I. Kaminer, *Coherent Interaction between Free Electrons and a Photonic Cavity*, Nature **582**, 50 (2020).
- [80] K. Soong, R. L. Byer, E. R. Colby, R. J. England, and E. A. Peralta, *Laser Damage Threshold Measurements of Optical Materials for Direct Laser Accelerators*, AIP Conference Proceedings **1507**, 511 (2012).
- [81] P. Li, A. Ruehl, U. Grosse-Wortmann, and I. Hartl, *Sub-100-Fs Passively Mode-Locked Holmium-Doped Fiber Oscillator Operating at 2.06  $\mu\text{m}$* , Optics Letters **39**, 6859 (2014).
- [82] P. Li, A. Ruehl, C. Bransley, and I. Hartl, *Low Noise, Tunable Ho:Fiber Soliton Oscillator for Ho:YLF Amplifier Seeding*, Laser Physics Letters **13**, 065104 (2016).
- [83] J. Breuer, R. Graf, A. Apolonski, and P. Hommelhoff, *Dielectric Laser Acceleration of Nonrelativistic Electrons at a Single Fused Silica Grating Structure: Experimental Part*, Phys. Rev. ST Accel. Beams **17**, 21301 (2014).

- [84] K. Brack, *Über Eine Anordnung Zur Filterung von Elektroneninterferenzen*, Z. Naturforsch. Teil A **17**, 1066 (1962).
- [85] M. S. Bronsgeest, Physics of Schottky Electron Sources, Dissertation thesis, TU Delft 2009.
- [86] N. Brodusch, H. Demers, A. Gellé, A. Moores, and R. Gauvin, *Electron Energy-Loss Spectroscopy (EELS) with a Cold-Field Emission Scanning Electron Microscope at Low Accelerating Voltage in Transmission Mode*, Ultramicroscopy **203**, 21 (2019).
- [87] D. Kreier and P. Baum, *Avoiding Temporal Distortions in Tilted Pulses*, Optics Letters **37**, 2373 (2012).
- [88] N. Ebrahim, S. T. D, T. Jau, and Z. Ahmed, *Four-Dimensional Imaging of Carrier Interface Dynamics in p-n Junctions*, Science **347**, 164 (2015).
- [89] E. Najafi, V. Ivanov, A. Zewail, and M. Bernardi, *Super-Diffusion of Excited Carriers in Semiconductors*, Nature Communications **8**, 15177 (2017).
- [90] K. J. Leedle, A. Ceballos, H. Deng, O. Solgaard, R. Fabian Pease, R. L. Byer, and J. S. Harris, *Dielectric Laser Acceleration of Sub-100 KeV Electrons with Silicon Dual-Pillar Grating Structures*, Optics Letters **40**, 4344 (2015).
- [91] E. Hecht, *Optics* (Pearson, 2012).
- [92] R. Dahan, S. Nehemia, M. Shentcic, O. Reinhardt, Y. Adiv, X. Shi, O. Be'er, M. H. Lynch, Y. Kurman, K. Wang, and I. Kaminer, *Resonant Phase-Matching between a Light Wave and a Free-Electron Wavefunction*, Nature Physics **16**, 1123 (2020).
- [93] T. W. Hughes, S. Tan, Z. Zhao, N. v Sapra, K. J. Leedle, H. Deng, Y. Miao, D. S. Black, O. Solgaard, J. S. Harris, J. Vuckovic, R. L. Byer, S. Fan, R. J. England, Y. J. Lee, and M. Qi, *On-Chip Laser-Power Delivery System for Dielectric Laser Accelerators*, Physical Review Applied **9**, 54017 (2018).
- [94] S. J. Smith and E. M. Purcell, *Visible Light from Localized Surface Charges Moving across a Grating*, Physical Review **92**, 1069 (1953).
- [95] I. M. Frank and V. L. Ginzburg, *Radiation of a Uniform Moving Electron Due to Its Transition from One Medium into Another*, Journal of Physics-Ussr **9**, 353 (1945).
- [96] R. Remez, A. Karnieli, S. Trajtenberg-Mills, N. Shapira, I. Kaminer, Y. Lereah, and A. Arie, *Observing the Quantum Wave Nature of Free Electrons through Spontaneous Emission*, Physical Review Letters **123**, 060401 (2019).
- [97] L. J. Wong, N. Rivera, C. Murdia, T. Christensen, J. D. Joannopoulos, M. Soljačić, and I. Kaminer, *Control of Quantum Electrodynamical Processes by Shaping Electron Wavepackets*.
- [98] D. C. Haynes, M. Wurzer, A. Schletter, A. Al-Haddad, C. Blaga, C. Bostedt, J. Bozek, H. Bromberger, M. Bucher, A. Camper, S. Carron, R. Coffee, J. T. Costello, L. F. DiMauro, Y. Ding, K. Ferguson, I. Grguraš, W. Helml, M. C. Hoffmann, M. Ilchen, S. Jalas, N. M. Kabachnik, A. K. Kazansky, R. Kienberger, A. R. Maier, T. Maxwell, T. Mazza, M. Meyer, H. Park, J. Robinson, C. Roedig, H. Schlarb, R. Singla, F. Tellkamp, P. A. Walker, K. Zhang, G. Doumy, C. Behrens, and A. L. Cavalieri, *Clocking Auger Electrons*, Nature Physics (2021).



## **Statement of the author's contribution to the publications**

All the publications selected for this thesis contain experimental, theoretical and numerical results to which I significantly contributed. The experiments described in these papers were performed during my postdoctoral fellowship in the group of prof. P. Hommelhoff in Erlangen, Germany. In the four sole author publications [A1,A10,A13,A15] I was responsible for all the parts of the research and data interpretation. In the publications [A2-A6,A9,A12] I contributed to the original idea behind the research. Further I was responsible for the development of the optical part of the experimental setup, the design of the nanostructures, the experiments and the interpretation of the data. In all cases I also contributed with the theory and numerical modelling of the observed effects. The publications [A7,A8] are based on my proposal to study the inelastic ponderomotive interaction between optical travelling waves and the electrons. For this purpose we developed a new setup based on pulsed scanning electron microscope with spectrally-resolved detection using a magnetic spectrometer (designed and fabricated by my bachelor student) and micro-channel plate detector. I was responsible for the setup development, the complete experimental part of these publications and also for data interpretation and manuscript writing. Publication [A11] summarizes the properties of the above-mentioned setup and I was involved in all parts of the research. In the publications [A12,A14] I designed the nanostructures using FDTD method and in [A12] I proposed the idea to use distributed Bragg reflectors to enhance the coupling of incident light to the synchronous evanescent mode.

## Appendix: Collection of publications

- [A1] M. Kozák, *Electron Acceleration in Moving Laser-Induced Gratings Produced by Chirped Femtosecond Pulses*, Journal of Physics B: Atomic, Molecular and Optical Physics **48**, 195601 (2015). DOI: 10.1088/0953-4075/48/19/195601
- [A2] J. McNeur, M. Kozák, D. Ehberger, N. Schönenberger, A. Tafel, A. Li, and P. Hommelhoff, *A Miniaturized Electron Source Based on Dielectric Laser Accelerator Operation at Higher Spatial Harmonics and a Nanotip Photoemitter*, Journal of Physics B: Atomic, Molecular and Optical Physics **49**, 34006 (2016). DOI: 10.1088/0953-4075/49/3/034006
- [A3] M. Kozák, J. McNeur, K. J. Leedle, H. Deng, N. Schönenberger, A. Ruehl, I. Hartl, H. Hoogland, R. Holzwarth, J. S. Harris, R. L. Byer, and P. Hommelhoff, *Transverse and Longitudinal Characterization of Electron Beams Using Interaction with Optical Near-Fields*, Opt. Lett. **41**, 3435 (2016). DOI: 10.1364/OL.41.003435
- [A4] M. Kozák, J. McNeur, K. J. Leedle, H. Deng, N. Schönenberger, A. Ruehl, I. Hartl, J. S. Harris, R. L. Byer, and P. Hommelhoff, *Optical Gating and Streaking of Free Electrons with Sub-Optical Cycle Precision*, Nature Communications **8**, 14342 (2017). DOI: 10.1038/ncomms14342
- [A5] M. Kozák, P. Beck, H. Deng, J. McNeur, N. Schönenberger, C. Gaida, F. Stutzki, M. Gebhardt, J. Limpert, A. Ruehl, I. Hartl, O. Solgaard, J. S. Harris, R. L. Byer, and P. Hommelhoff, *Acceleration of Sub-Relativistic Electrons with an Evanescent Optical Wave at a Planar Interface*, Optics Express **25**, 19195 (2017). DOI: 10.1364/OE.25.019195
- [A6] M. Kozák, M. Förster, J. McNeur, N. Schönenberger, K. Leedle, H. Deng, J. S. Harris, R. L. Byer, and P. Hommelhoff, *Dielectric Laser Acceleration of Sub-Relativistic Electrons by Few-Cycle Laser Pulses*, Nuclear Instruments and Methods in Physics Research Section A: Accelerators, Spectrometers, Detectors and Associated Equipment **865**, 84 (2017). DOI: 10.1016/j.nima.2016.12.051
- [A7] M. Kozák, T. Eckstein, N. Schönenberger, and P. Hommelhoff, *Inelastic Ponderomotive Scattering of Electrons at a High-Intensity Optical Travelling Wave in Vacuum*, Nature Physics **14**, 121 (2018). DOI: 10.1038/NPHYS4282
- [A8] M. Kozák, N. Schönenberger, and P. Hommelhoff, *Ponderomotive Generation and Detection of Attosecond Free-Electron Pulse Trains*, Physical Review Letters **120**, 103203 (2018). DOI: 10.1103/PhysRevLett.120.103203
- [A9] J. McNeur, M. Kozák, N. Schönenberger, K. J. Leedle, H. Deng, A. Ceballos, H. Hoogland, A. Ruehl, I. Hartl, R. Holzwarth, O. Solgaard, J. S. Harris, R. L. Byer, and P. Hommelhoff, *Elements of a Dielectric Laser Accelerator*, Optica **5**, 687 (2018). DOI: 10.1364/OPTICA.5.000687
- [A10] M. Kozák, *Nonlinear Inelastic Scattering of Electrons at an Optical Standing Wave*, Physical Review A **98**, (2018). DOI: 10.1103/PhysRevA.98.013407
- [A11] M. Kozák, J. McNeur, N. Schönenberger, J. Illmer, A. Li, A. Tafel, P. Yousefi, T. Eckstein, and P. Hommelhoff, *Ultrafast Scanning Electron Microscope Applied for Studying the Interaction between Free Electrons and Optical Near-Fields of Periodic Nanostructures*, Journal of Applied Physics **124**, 023104 (2018). DOI: 10.1063/1.5032093
- [A12] P. Yousefi, N. Schönenberger, J. McNeur, M. Kozák, U. Niedermayer, and P. Hommelhoff, *Dielectric Laser Electron Acceleration in a Dual Pillar Grating*

- with a Distributed Bragg Reflector*, Optics Letters **44**, 1520 (2019). DOI: 10.1364/OL.44.001520
- [A13] M. Kozák, *All-Optical Scheme for Generation of Isolated Attosecond Electron Pulses*, Physical Review Letters **123**, 203202 (2019). DOI: PhysRevLett.123.203202
- [A14] H. Deng, K. J. Leedle, Y. Miao, D. S. Black, K. E. Urbanek, J. McNeur, M. Kozák, A. Ceballos, P. Hommelhoff, O. Solgaard, R. L. Byer, and J. S. Harris, *Gallium Oxide for High-Power Optical Applications*, Advanced Optical Materials **8**, 1901522 (2020). DOI: 10.1002/adom.201901522
- [A15] M. Kozák, *Electron Vortex Beam Generation via Chiral Light-Induced Inelastic Ponderomotive Scattering*, ACS Photonics **8**, 431 (2021). DOI: 10.1021/acsp Photonics.0c01650